THE ELECTRO-MAGNETIC PROPERTIES OF COMBINED CARBON NANOTUBES AND CARBON-COATED IRON NANOPARTICLES-MODIFIED POLYMER COMPOSITES

by

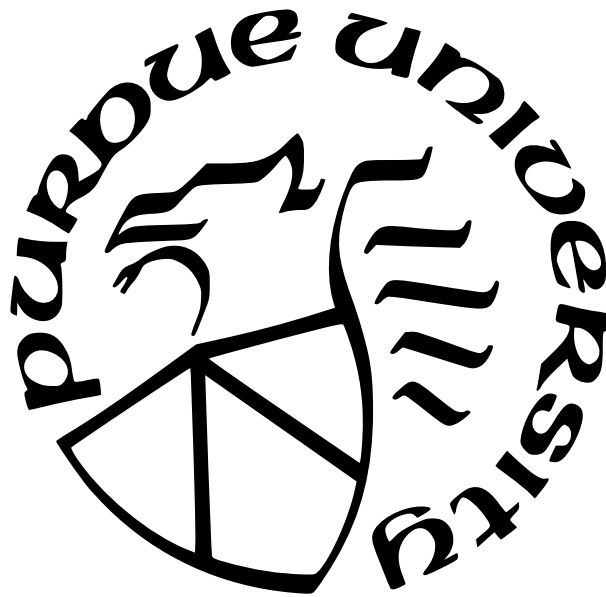**Jassimran Kaur Arora**

A Thesis

Submitted to the Faculty of Purdue University

In Partial Fulfillment of the Requirements for the degree of

Master of Science

School of Aeronautics and Astronautics

West Lafayette, Indiana

August 2023

THE PURDUE UNIVERSITY GRADUATE SCHOOL
STATEMENT OF COMMITTEE APPROVAL

Dr. Tyler N. Tallman, Chair

School of Aeronautics and Astronautics

Dr. Vikas Tomar

School of Aeronautics and Astronautics

Dr. Fabio Semperlotti

School of Mechanical Engineering

Approved by:

Dr. Gregory A. Blaisdell

To my parents, friends, mentors and colleagues

ACKNOWLEDGMENTS

I would like to express my deepest gratitude and appreciation to all those who have supported me throughout my journey in completing this Masters thesis. Without their unwavering encouragement, guidance, and assistance, this accomplishment would not have been possible.

First and foremost, I am indebted to my supervisor, Dr. Tyler Tallman, for his invaluable support and expertise. His guidance, patience, and insightful feedback played a crucial role in shaping this research project.

I would also like to extend my sincere thanks to the members of my thesis committee, Dr. Vikas Tomar and Dr. Fabio Semperlotti, for their time and valuable input. Their constructive criticism has significantly enhanced the quality of this work.

I am deeply grateful to my parents for their unwavering support, the staff and faculty members at Purdue University, whose knowledge and expertise have been instrumental in shaping my academic journey. I would like to acknowledge the efforts of Dr. Neil R. Dilley, Brandon Stevens, and Dr. Christopher J. Gilpin who provided valuable assistance in accessing relevant resources and materials.

Furthermore, I would like to express my heartfelt appreciation to my mentor, Julio Hernandez, my uncle and aunt in Texas, and friends I made in West Lafayette and at Purdue for their unwavering support and encouragement. Their love, understanding, and motivation were vital in keeping me focused and motivated during the challenging times. Lastly, I would like to thank Mohit Sukhija for his depth of support.

To everyone who has played a part, big or small, in my pursuit of knowledge and the completion of this thesis, I extend my deepest gratitude. Your support and belief in me has been truly inspiring. Thank you for being a part of this important milestone in my academic journey.

TABLE OF CONTENTS

LIST OF TABLES

LIST OF FIGURES

ABBREVIATIONS

AC	alternating current
CB	carbon black
CCFeNP	carbon-coated iron nanoparticles
CF	carbon fiber
CFRP	carbon-reinforced polymer
CNF	carbon nanofiber
CNT	carbon nanotubes
DC	direct current
DMM	digital multimeter
EIS	electrical impedance spectroscopy
FeMWNT	Fe-filled multi-walled carbon nanotubes
FGM	functionally graded material
GCE	glassy carbon electrod
GNP	graphene nanoplatelets
MFMS	multifunctional material systems
MNC	magnetic nanocomposite
MPMS	magnetic property measurement system
MRE	magnetorheological elastomer
MRI	magnetic resonant imaging
MWCNT	multi-walled carbon nanotubes
NNCF	nickel coated carbon fiber
PDMS	polydimethylsiloxane
PMC	polymer matrix composites
PMMA	polymethyl methacrylate
SEM	scanning electron microscope
SQUID	superconducting quantum interference device
TEM	transmission electron microscope
VSM	vibrating sample mode

ABSTRACT

Polymer based multifunctional material systems (MFMS) have gained increasing attention in the past two decades. The addition of nanofillers and nanoparticles allows for modification of physical properties as well as the discovery of new features. Multifunctionalization of composites allows us to "do more with less". For example, electrically conductive additives can eliminate the need for sensors through self-sensing principles, shape morphing matrices can reduce the need for actuators, and the inclusion of fire-resistant constituents can reduce flammability in stringent fire protection measures. With added capabilities, the applications of multifunctional composites extends beyond the aerospace and automotive industries to healthcare, infrastructure, electronics, among others, and optics.

The current state of the art is largely focused on single-filler composites or multifiller composites with complementary attributes. For example, carbon nanotubes (CNTs) when mixed with graphene produces higher conductivity than can be achieved via modification with either CNTs or graphene alone. The majority of investigations conducted in this domain have fillers selected with the aim of imparting a singular property. Much less has been done in the area of multifiller and multifunctional polymer matrix composites (PMCs) which can exhibit multiple properties. Consequently, this work seeks to contribute towards the field of *synergistic* functional composites. That is, a multifiller composite material system comprised of differently functional fillers. This approach has potential to yield smart material systems that outperform single-filler or single-functionality materials through the discovery of novel synergistic coupling between the differently functional phases.

In light of the preceding motivation, this work presents the results on the experimental electromagnetic and mechanical characterization of multi-walled carbon nanotubes (MWCNTs) + carbon-coated iron nanoparticle (CCFeNP)-modified polymers. Carbon nanotubes with their electrical properties and iron nanoparticles with their magnetic attributes present potential for synergistic electromagnetic interactions in a well-percolated network. We report on the electro-magnetic properties of MWCNT + CCFeNP/epoxy composites including DC and AC conductivity, dielectric permittivity, magnetic permeability, and piezoresistance as a function of varying relative MWCNT and CCFeNP concentrations. The results are

in a large part linked to the manufacturing process described herein. This work seeks to establish the foundations of synergistic functional filler combinations that could lead to new multifunctional capabilities in the future.

1. INTRODUCTION

During the early stages of aviation, aircraft were primarily constructed using a natural composite material known as wood, in conjunction with wire and fabric. However, in the 1930s, aluminium alloys emerged as a dominant force and have maintained that position since. Currently, the industry is focused on replacing secondary members in aerial vehicles and aerospace structures with composites. The decision to transition from traditional materials to more advanced fiber-based composites is driven by several factors, including their high tensile strength, superior stiffness, and excellent durability. And of all the available options to choose from, a thermosetting epoxy system was the engineering community's top choice for the matrix material. This is largely because of its higher resistance to environmental degradation. Notable examples of the considerable impact of composites in this regard are the Boeing 757, 767, and 777 and the Airbus A310, A320, A330, and A340 airliners[1].

The preceding example illustrates only one of the many ways polymer based composites have been integrated into our daily lives. When these polymer based composites offer more than just structural benefits, we can call them multifunctional materials. Multifunctional material systems can be defined as materials that possess *multiple* desirable engineering characteristics (e.g., electrical, thermal, magnetic, optical, mechanical or other properties). The inclusion of multiple desirable properties in one eliminates the need for auxiliary components in complex electromechanical systems. This often reduces the total mass and volume of the system and thereby increases efficiency. These characteristics expand the scope of applications of a single material to myriad domains. Some examples include wearable healthcare devices[2], structural health monitoring[3], heating and ventilation[4], and detection of toxic gases for safety purposes[5]. Designing multifunctional composite materials and structures is a challenging task because the combination of materials and the fabrication process play a crucial role in impacting the functional capabilities of the final product. These materials have applications that can span structural or non-structural domains or sometimes even a combination of the two. It should be noted here that the meaning of "multifunctional materials" is not well defined in prior work. Some authors choose to use the term "smart/intelligent material" in place of multifunctional materials. For the purposes of this work, MFMS refers

to multifunctional composites. According to the current state of the art, most work involves integrating different types of functional devices and/or additives to manufacture these materials. For example, embedded sensors that measure strain and/or temperature changes to localize damage have been developed. Embedded sensing is usually done through fiber optics[6] or via piezoelectric sensors and actuators[7]. Nanofillers have also been extensively studied for the advantages they offer when combined with a bulk matrix. These include electrical conductivity[8], electrolytic properties[9], permittivity[10], optical properties[11], and ion selectivity[12]. While most research is focused on adding only one type of functional property to the matrix, some work has been done to combine fillers that could potentially produce a material system with multiple functionalities. That is, multifiller multifunctional materials have been developed where the fillers interact to impart one or more desirable qualities to the system. Some examples of both are discussed in the following sections.
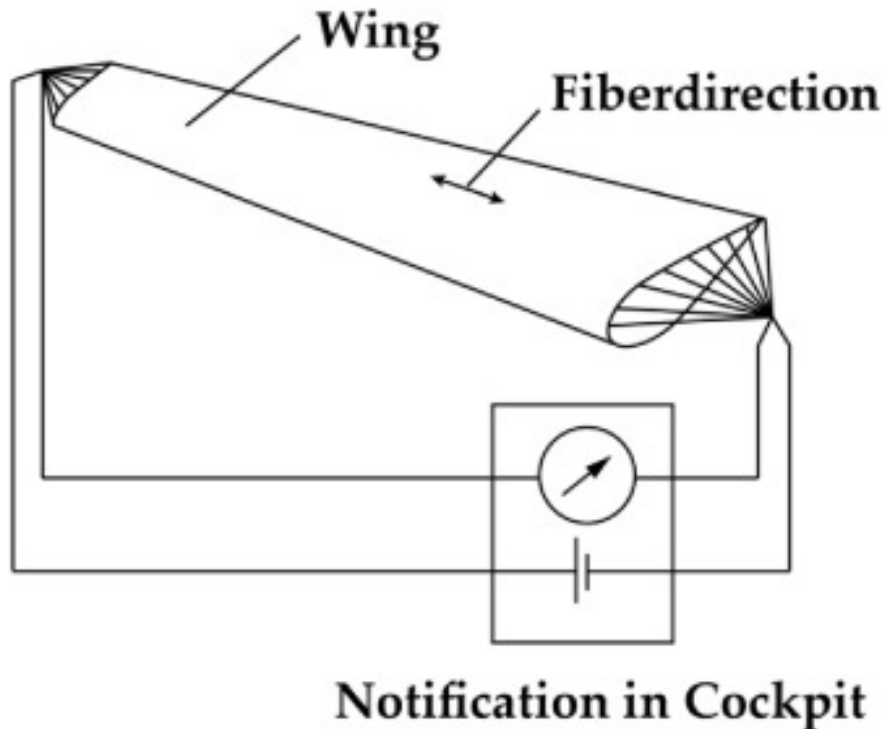
Figure 1.1. Layout of an airplane wing-mounted state monitoring sensor [13].

1.1 Single-filler multifunctional materials

We shall first look at nanomaterial based MFMS. Nature offers various allotropes of carbon because of its co-valency. Scientists have taken advantage of its stability to develop carbon based nanoparticles in the form of tubes, cones, spheres, and sheets. These include graphene, CNTs, carbon black (CB) and carbon nanofibers (CNFs). Carbon has been the choice of filler for various applications in MFMS because of its great mechanical, thermal, and electrical properties[14], [15]. These properties have endowed the filler with many functions like actuation[16], energy storage[17], strain and chemical sensing[18], energy harvesting[19], corrosion protection, flame retardancy and environmental protection[20]. The piezoresistivity of carbon based polymer nanocomposites has been much studied because of its diverse applications. These include strain sensing[21], measurement of blood pressure in the medical field[22], electronic textiles[23], and pressure sensing in the automotive industry[24].
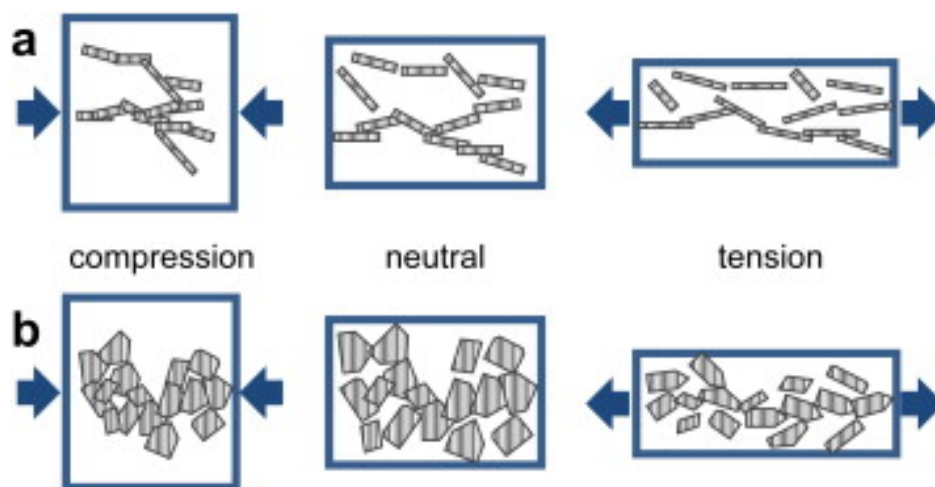
Figure 1.2. Schematic illustration of piezoresistivity induced by carbon nanofillers: (a) carbon naotubes 1-D filler; and (b) graphene 2-D filler.[25]

Another category of multifunctional materials are functionally graded materials (FGMs). These materials are also made of a matrix and a reinforcement material. However, the matrix is usually metallic (Al, Cu, Mg, Ti, and Ni) and the reinforcements are usually ceramics at the micron scale (SiC, CNT, Al_2O_3, TiB_2, SiO_2, and ZrO_2)[30]. These systems are manufactured in a manner so as to achieve spatial variations in composition and/or microstructure. This
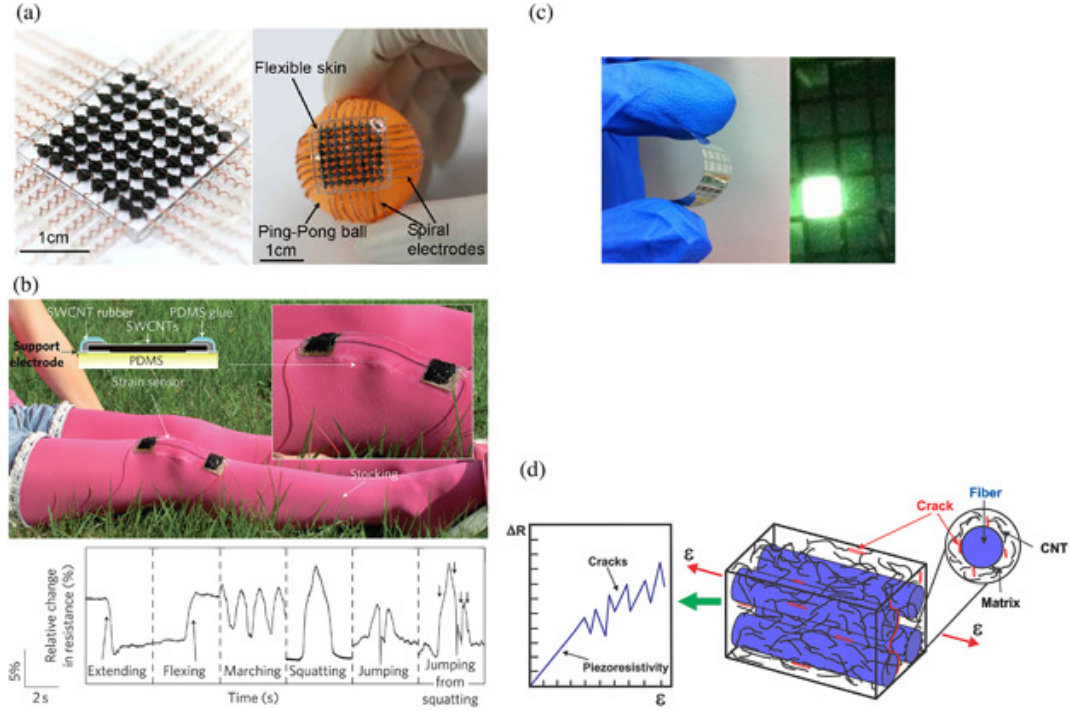
Figure 1.3. Applications of piezoresistive polymer nanocomposites based on carbon nanostructures. a) Highly twistable tactile sensing array made from polydimethylsiloxane (PDMS) and carbon black nanoparticles[26], b) Stretchable single wall CNT/PDMS strain sensor for human motion detection[27], c) Organic light-emitting diode on a graphene/polymethyl methacrylate (PMMA) transparent conducting electrode[28], and d) Schematic showing the use of carbon nanotubes in a polymer matrix to self-sense crack propagation and damage in advanced multiscale composites[29].

allows scientists to control thermal, structural or other functional properties. The gradation of properties makes the material more resistant to thermal and mechanical stress concentrations one would expect in traditional composites[31]. Originally developed for thermal barrier purposes in fusion reactors and aerospace structural applications, FGMs have since found utility in high-temperature structural components[32]. They can also potentially be used for chemical sensing, rocket nozzles[31], solar cells[33], artificial bones[34], nanopipes, nanoreactors, actuators, engine cylinders, brake rotors, probes, leaf springs, gas adsorbents[35], sonar domes, and catalyst supports among others[36].

Next, we shall look at polymeric carbon fiber (CF) based structural composite materials. Conductive structural composites generally consist of two phases: a reinforcing fiber

and a matrix. Smart structural composites that are multifunctional include added functions like strain and stress sensing[37], damage detection[38], thermoelectric energy generation[39], electro-magnetic interference shielding[40], current rectification, self-healing[41], and noise and vibration control[42]. The sensing capability of a carbon fiber based sensor can be enhanced if the matrix material is conductive[43]. This can be done by adding conductive particles (CNFs, CNTs, GNPs, etc.). In addition to good structural and electrical properties, the conductive network of carbon fiber can be leveraged for its resistance heating as well. Schulte and Baron[13] showed that Joule heating can modify the mechanical properties of carbon fiber reinforced polymer (CFRP) based structures and thereby affect the fiber's environment. Joule heat can be produced by direct current injections that locally heats the surrounding environment of the fiber. Joseph and Viney[44] harnessed this phenomenon to successfully produce epoxy based carbon fiber composites. This was done by clustering CFRP prepregs between copper blocks and then heating the setup up to the temperature needed for crosslinking by a current injection. Resistance heating finds an application in the welding of thermoplastic polymer matrix composites as well[45].

Conductive structural materials can also be employed for energy applications. Structural capacitors have emerged as a form of advanced energy storage[17]. The inclusion of multifunctional composite materials (i.e., CFRP) broadens the scope of applications to include structural domains. Thus, multifunctional composites used as energy storage devices could offer both enhanced electrical as well as mechanical properties. This integration also facilitates considerable space savings[47]. Additionally, conductive nanoparticles (metallic powders or carbon-based nanofillers) can also enhance dielectric permittivity of capacitors[48].

Magnetic nanocomposites (MNCs) have also drawn increased attention thanks to their remarkable properties. They typically contain magnetic nanoparticles that respond to external stimuli, that is, a static or alternating magnetic field. The resultant magnetomechanical forces finds practical applications in many fields like actuation[49], drug delivery[50] or even magnetic separation[51]. Additionally, in the presence of external magnetic fields, magnetic particles can behave like nanoheaters[52] which can be leveraged for biomedical applications[53]. Some prior work utilizes core-shell MNCs. That is, the structure comprises of a magnetic core which is usually coated with a metal. The shell acts as a shield to pro-
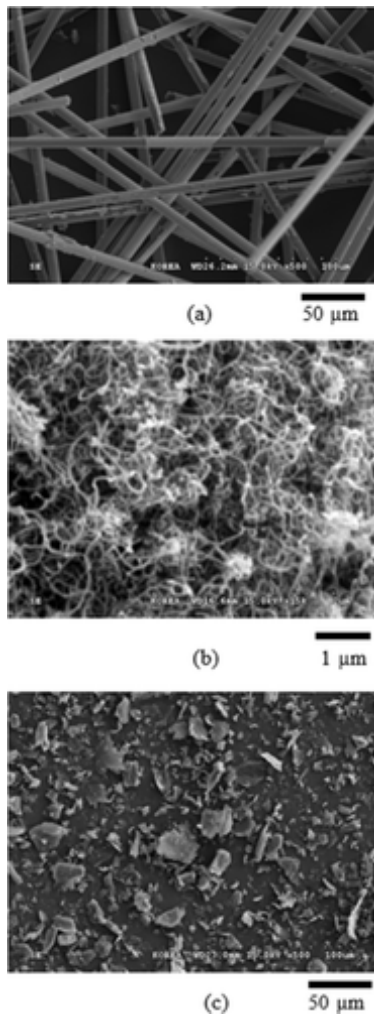
Figure 1.4. Scanning electron micrographs of the conductive fillers used in this study: (a) Ni-coated carbon fiber (NCCF), (b) multi-walled carbon nanotubes (MWCNTs), (c) graphite[46].

tect the core from further oxidation and corrosion. Sometimes silica is chosen as the shell material for magnetic cores. This material aids particle dispersion, enhances thermal and chemical stability, decreases toxicity, and offers good microwave absorption[54], [55]. Carbon coated magnetic nanocomposites[56] have also emerged as a material choice in the realm of sensing and actuation. Similar to the metallic shell discussed above, the carbon shell acts as a physical barrier to hinder particle aggregation. Additionally, the hydrophillic coating can be of interest as drug carriers for magnetic resonant imaging (MRIs)[57] and drug therapy[58]. Other representative applications include water purification[59], sensing[60], tu-

19

mor apoptosis[61], and biomolecule separation[62]. Applications of MNCs in electronics are illustrated in Figure 1.5. There are numerous untapped applications in various domains for novel combinations of magnetic particles and host materials.
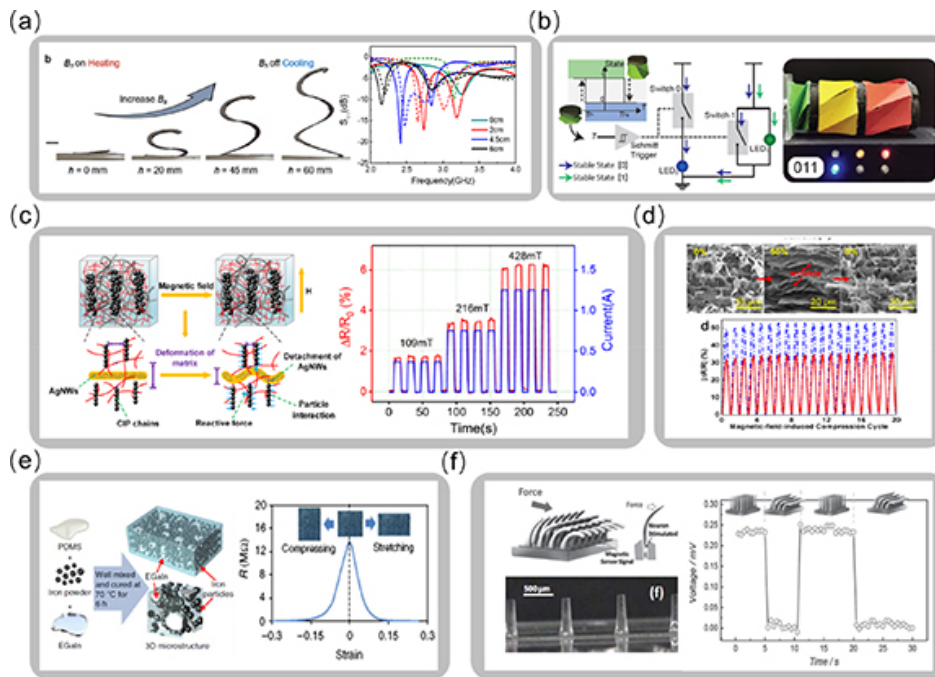
Figure 1.5. Configurable electronics and sensors via multiphysics coupling of magnetic soft composites. (a) Configurable antenna with an actively tunable resonant frequency[63], (b) Multifunctional magneto-mechano-electric origami assembly for digital computing[64], (c) Magnetically responsive soft material sensor by embedding silver nanowires in MRE[65], (d) Self-sensing magnetic graphene aerogel with strain-dependent resistance[66], (e) Magnetically responsive soft material sensor embedding liquid metal in MRE[67], (f) Deformation sensor mimicking cilium structure[68].

1.2 Multifiller nanocomposites with complementary properties

Scientists have successfully developed a wide variety of particulates/flakes and fibers to chose from when it comes to modifying thermosetting and thermoplastic matrices. According to Wypych[69], more than 70 types of the former and more than 15 types of the latter are widely available for use. While previous work has explored the affect of each additive in a PMC individually, scientific curiosity has also led researchers to combine some of them and

analyze the combined material system. This has led to the development of "hybrid composites". Different researchers have chosen to define this term differently. Thwe and Leo[70] described this as a combination of different matrices with a single reinforcing material. On the other hand, Fu et al.[71] use this term to define a system containing more than one filler in a single matrix. For the purpose of this work, we are focused on a hybrid composite made up of more than one type of filler in a single polymer base. Hybrid nanocomposites are expected to exhibit new characteristics that may or may not be inherent to the individual components. A hybrid composite is also vastly different from a hybrid material because the properties of a hybrid material can be modelled as a combination of the properties of the constituent materials (e.g., the rule of mixtures). The same cannot be said for hybrid nanocomposites because the factors influencing the properties of the system are vastly different (interfacial interactions between different fillers or fillers and the matrix). Researchers use the term "synergy" to define the interaction of the components in these systems. This is due to the synergistic effect generated by their combination. The collective impact of fillers surpasses the cumulative effects of the individual constituents. In other words, synergy refers to the interaction of elements wherein each component enhances the effectiveness of the others when combined[72].

Presently, significant emphasis is placed on complementary conductive multifiller composites, aiming to harness a synergistic impact through the utilization of two or more carbon fillers possessing distinct geometries and electrical properties. This focus arises from the abundant availability of conductive fillers. Complementary effects are considered particularly important below the percolation threshold. A combination of conductive fillers can show conductive characteristics even when the concentration of each lies below the percolation threshold of each filler[74]. The significant attention directed towards conductive polymer composites stems from their wide-ranging utilization in various domains, including but not limited to anti-static materials, electromagnetic shielding, conductive films, conductive coatings, and phase-transfer catalysis.[75]–[77]. Ma et al.[8] explored the capabilities of the carbon black-multi-walled carbon nantube (CB-MWCNT) system as a hybrid filler for epoxy based nanocomposites. Different types of nanocomposites were manufactured: CB-only, CNT-only, and others by adding varying amounts of CB to either 0.2 wt.% CNT or 0.4 wt.% CNT. The
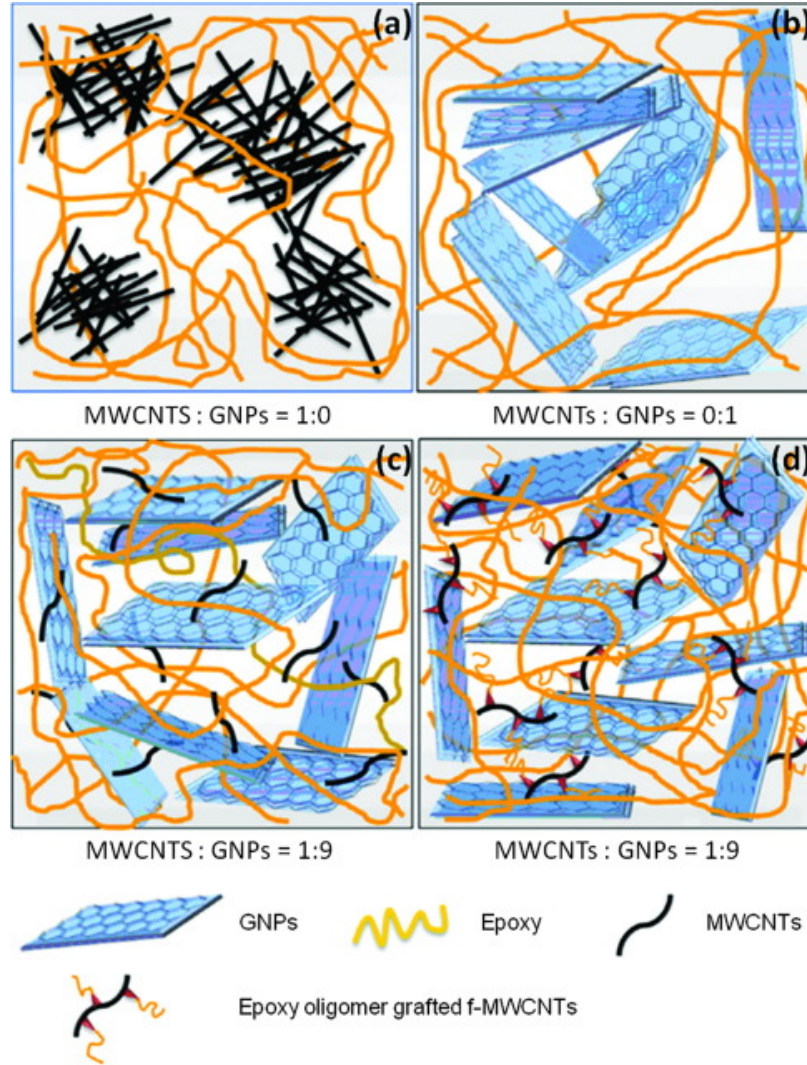
Figure 1.6. Model of the microstructural network in epoxy composites with various weight ratios of MWCNTs and GNPs[73].

hybrid systems displayed better DC characteristics when compared against the single-filler composites. The addition of 0.2 wt.% CB particles to 0.2 wt.% CNTs led to a significant enhancement in electrical conductivity, increasing by approximately six orders of magnitude. Apart from enhancing the electrical conductivity of the composites, the incorporation of CB particles yielded notable improvements in the plasticity and fracture strength of the CNT/CB hybrid nanocomposites. This finding highlights the synergistic effect achieved by CB in conjunction with CNT. We can say that both the carbon based fillers were acting

in a complementary manner. That is, the fillers worked together to augment the electrical conductivity than could be achieved by either CNTs or CB alone.
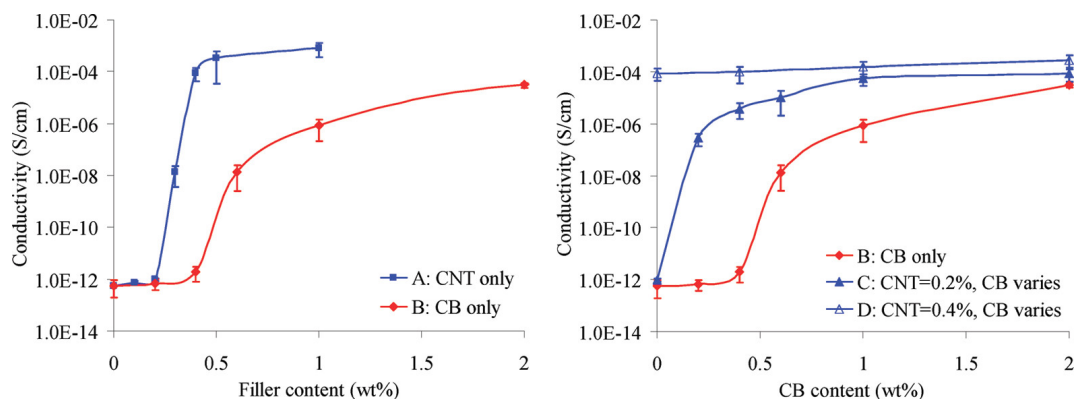
Figure 1.7. DC electrical conductivities of nanocomposites containing either CNT or CB alone and fixed CNT contents of 0%, 0.2%, and 0.4% plus varying CB contents[8].

Another example of complementary fillers are graphene or functionalized graphene and CNTs. The amalgamation of these additives has exhibited synergistic effects in terms of enhanced tensile strength, improved thermal and electrical conductivities[78], as well as increased supercapacitance[73]. Graphene (with its two-dimensional geometry) has undeniable advantages: high aspect ratio[79], good electrical conductivity, and high sensitivity. Thus, the combination of graphene with one-dimensional CNTs puts forth the possibility of promising complementary composite systems. Li et al.[80] investigated the electrical and mechanical characteristics of a hybrid epoxy nanocomposite made of MWCNTs and graphite nanoplatelets (GNPs). They also fabricated single and two-filler composites: CNT/epoxy, GNP/epoxy and by incorporating varying weight fractions of MWCNTs into GNP from 0.1 wt.% to 1 wt.%. For the multi-filler composite, the maximum total filler weight fraction was held constant at 2 wt.%. When comparing the electrical conductivity of the mixed-filler specimens against the GNP-only specimens, it was discovered that for the same weight fraction of fillers, the former had better conductive properties than the latter. Additionally, the fracture toughness of the hybrid system was 21% higher than it single-filler counterpart. This was attributed to crack tip bridging and CNT pullout. Similar studies have been conducted in thermosetting polymers as well[81], [82].
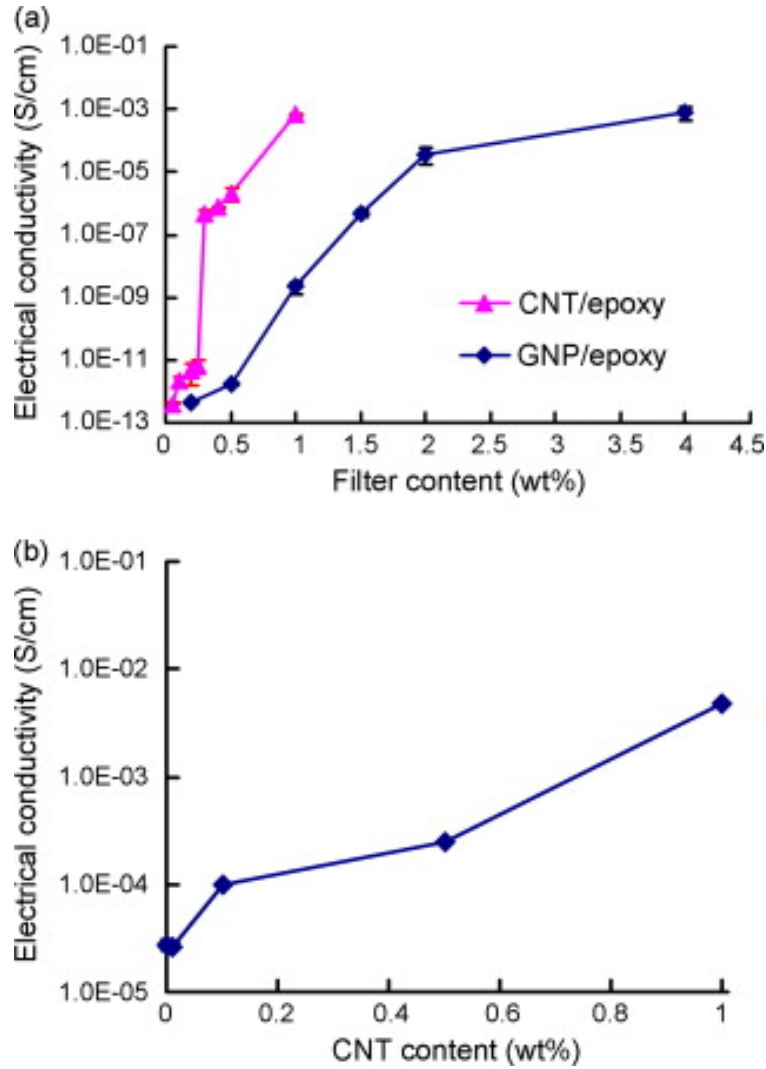
Figure 1.8. Electrical conductivity of (a) CNT or GNP nanocomposites as a function of filler content and (b) 2 wt.% CNT/GNP hybrid nanocomposites as a function of CNT content[80].

1.3   Carbon + iron based composites

As discussed previously, carbon based inclusions can develop a well-connected electrical network in an insulating matrix. Similarly, ferromagnetic particle have shown to impart magnetic permeability to the same. One would expect a combination of the two to introduce both electrical and magnetic functionality in a polymer. Some work has been done to combine conductive ferromagnetic fillers ($BaTiO_3$, Fe, Ni) with conductive carbon fillers (CNTs, CB) and analyze the resulting system. This thesis is focused on one such combination of magnetic

and electrical fillers, MWCNT + CCFeNP. And thus, it is worth exploring the current state of the art. Some of our findings are discussed below.

For example, Lozitsky et al.[83] explored the electrical properties of epoxy containing CNT and inorganic fillers: carbonyl iron (Fe) and titanium dioxide (TiO_2) particles. The concentration of titanium dioxide was fixed at 35 wt.% and that of iron was fixed at 30 wt.%, respectively. The concentration of CNTs was varied from 1 wt.% to 5 wt.% in increments of 1 %. To understand the effect of TiO_2 and Fe, the results were compared against CNT only composites. The DC conductivity curves indicate that the addition of TiO_2 or Fe lowers the conductivity when CNT is less than 3 wt.% and increases it beyond 3 wt.%. It was hypothesized that at low weight fractions, the presence of ferromagnetic fillers impedes the development of a conductive network within the matrix. However, beyond 3 wt.%, the electro-conductive Fe particles supposedly act as "bridges" between CNT particles, effectively reducing the distance between conductive particles. The AC conductivity of the Fe hybrid system indicates that beyond 3 wt.% CNT, the effect of increasing frequency is minimal. The real permittivity values of the multi-filler composite increased with increasing CNT content. This phenomenon was attributed to the increased polarization of conductive clusters of similar elements (CNT-CNT), dissimilar elements (CNT-Fe), and interfacial polarization at the filler-polymer junctions. While this paper establishes results in electrical conductivity, it fails to explore the effect of magnetic fillers on conductivity, that is, magnetoresistance.
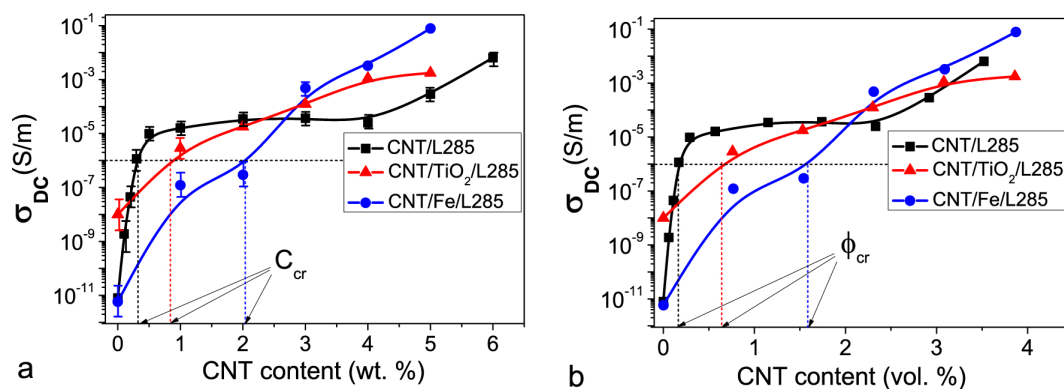
Figure 1.9. DC conductivity of CNT/L285, CNT/TiO2/L285 and CNT/Fe/L285 versus CNT content in wt% (a) and vol.% (b)[83].

Hudziak et al.[84] manufactured Fe-filled carbon nanotubes (Fe-MWNT) and suspended them in a polyurethaneurea matrix. Electrical conductivity tests on rectangular films of this material exhibited a percolation threshold at 0.35 wt.% filler concentration. Stress-strain measurements performed on unloaded and 10 wt.% FeMWNT-loaded samples yielded the Young's moduli at 10 MPa and 25 MPa, respectively. The material system was also subjected to strain dependent magnetoresistance testing. The FeMWNT composites exhibited magnetoresistance which could be a consequence of the interaction of the applied magnetic field and the ferromagnetic domains in the FeMWNT core. A sudden jump in magnetoresistance was observed at low axial strain (up to 20%). In the presence of an applied magnetic field, dipoles in the iron are expected to experience a magnetic torque. This would cause preferential orientation of the conducting nanotubes perpendicular to the axial current flow. Thus, the conduction pathway would be broken. This work was focused on the magnetoresistive response of a mechanically-loaded hybrid elastomer composite.
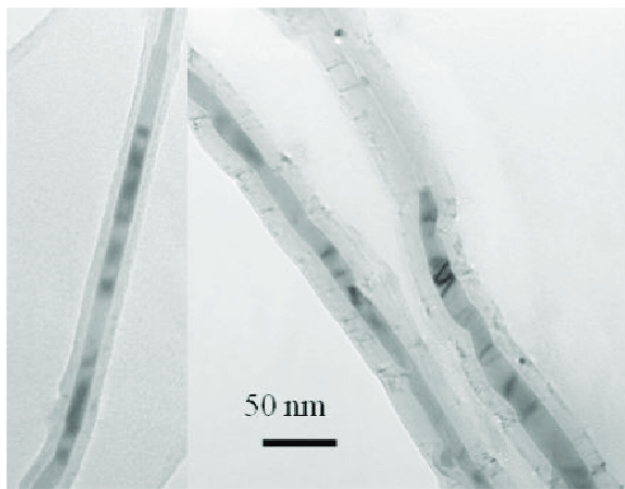
Figure 1.10. TEM micrographs of individual FeMWNTs extracted from the deposits[84].

Engel et al.[85] synthesized a single-walled carbon nanotube (SWCNT)-iron oxide nanocomposite and studied the resulting antimicrobial activity and magnetic response of the material. Bactericidal results on two strains of E. coli indicated that the material system is capable of serving as an antimicrobial agent for the disinfection of polluted waters. It was also discovered that the nanocomposite is reuasble in this application when washed with calcium chloride and distilled water. However, the efficiency of its performance drops when
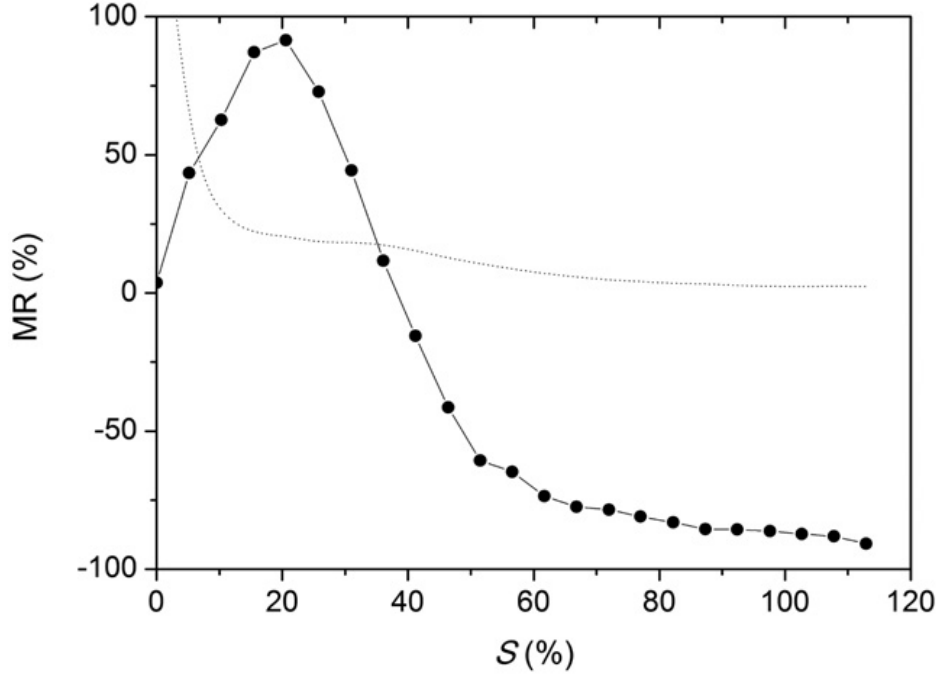
Figure 1.11. Magnetoresistance, versus axial strain. The dotted line is the variation of the derivative of R60 with respect to axial strain expressed as a percentage of R60.[84].

washed more than four times. Thermograms on iron oxide-only, SWCNT-only and hybrid nanocomposites indicated that the thermal degradation temperature of the hybrid system lies between the single-filler systems. The iron-only specimens showed no degradation at all. The hysteresis loops show that the iron oxide-SWCNT system has a lower saturation magnetization than the iron-only specimens. This paper was largely centered around the anti-bacterial properties of a mixed carbon-iron nanocomposite.

Mousavi et al.[86] modeled the nanocomposite of carbon nanotube and α-Fe_2O_3, using molecular mechanics and semi-empirical methods. This work was centered around the electrochemical compatibility of the nanocomposite for coating on a glassy carbon electrode (GCE). This work was also motivated by the application of this material system as a counter electrode in dye-sensitized solar cells. Results showed good availability of surface area for electroactivity, low peak-to-peak separation, superb current density, high response stability, and low resistance due to the high electrical conductivity and the remarkable electrocatalytic ability of the MWCNT/α-Fe_2O_3 electrode material.

1.4 Motivation

The numerous examples discussed above have covered extensive ground in the area of single-filler and multifiller multifunctional modified polymers. While single-filler composites were born from a need to impart different types of desirable characteristics to polymers, hybrid composites remain largely conductive. Most work in the realm utilizes complementary fillers to produce systems with good electrical properties at low filler concentrations. Some work has been done to combine the functionality of electrical and magnetic fillers. Combining these fillers has the potential to produce a smart material that is more than the sum of its constituents. That is, it has the potential to exhibit both electrical and magnetic properties. This could also be called a *synergistic* composite since the functionality of the composite is dependent on the multi-physical interplay of different parts within it. A lot of prior work uses the term *synergy* to describe nanocomposite systems with two or more nanofillers contributing towards a single multifunctional property. It is necessary to note here that the authors of this work will use this term differently. All references to synergistic functionality in this document imply a single composite modified with two or more different functional nanofillers, the multi-physical interactions of which give rise to new functional properties. That is, a material system with multiple types of nanoparticles that possesses properties not achievable by single additive alone but arises as a result of the interplay of some or all additives.

The current state of the art discussed here has illuminated a gap in the field of *synergistic* electro-magnetic composites. Work done to combine iron and carbon often uses oxidized iron (Fe_2O_3, Fe_3O_4)[87], modifies the structure of the fillers[88], or is centered around a specific application[89]. It was discovered that little to no work was done to establish the baseline synergistic characteristics of a multifiller electro-magnetic composite that employs unmodified MWCNTs and Fe. Additionally, the material system developed herein employs iron nanoparticles which are protected from oxidation by a carbon coating. Unoxidized iron has vastly different magnetic characteristics than oxidized iron. This thesis encompasses various electrical properties (conductivity, permittivity), magnetic properties (permeability), as well as mechanical properties (piezoresistance).

2. PROBLEM STATEMENT, RESEARCH GOAL, AND NOVEL CONTRIBUTIONS

2.1 Problem Statement

Despite the widespread use of modified polymer composites, the realm of electro-magnetic multifunctional nanofiller-modified polymer matrix composites (PMCs) is dominated by one of two groups: PMCs modified with only a single type of nanofillers or PMCs modified with multiple types of nanofillers acting in a complementary manner. These works are usually predominantly focused on modifications using a single type of filler or a combination of fillers to achieve a solitary functional property. Therefore, the **gap in the state of the art** is that limited efforts have been made towards modifying composites with multiple differently functional filler types that will endow the composite with multiple distinct characteristics. Addressing this gap is important because it can significantly expand the application space of multifunctional materials.

2.2 Research Goal

The **research goal** of this work is to study multifunctional PMCs modified with multiple types of fillers chosen for potential synergistic interactions. That is, manufacture and characterize a composite with functional properties not achievable by any single filler phase but that emerge as a result of the interplay of the fillers. In the context of this work, *synergistic functionality* refers to the incorporation of two or more nanofillers with distinct functional characteristics into a single composite, where their multi-physical interactions synergistically generate novel functional properties. This is significantly different from the prevailing state of the art that uses synergy to define multifiller composites where most or all phases contribute to a property that is achievable (although often to a lesser extent) by either phase individually.

2.3 Novel Contributions

The exploration of this concept is expected to stimulate advancement in the state of the art by unlocking distinctive functional properties in multi-filler composites. Consequently, it can broaden the design possibilities and potential applications of functional composites. Through this work, the author lays the groundwork in synergistic functionality between multi-walled carbon nanotubes and carbon-coated iron nanoparticles. This unique pair of nanofillers are expected to produce unique synergistic effects like adaptable electro-magnetic properties on demand, as well as the presence of multi-physical intrinsic self-sensing capabilities. While the focus of this study is on a particular material system, the fundamental insights, methodologies, and instrumentation developed herein are expected to have broad applicability across diverse and exciting domains of synergistically functional materials.

2.4 Document Structure

First, the experimental section dives into the manufacturing and various test methods deployed to produce and characterize the behavior of CNT + CCFeNP composites. Next, it presents a look at the results from the various tests and interprets the multi-physical interactions. The thesis wraps up with a summary, conclusions, and review of future work.

3. EXPERIMENTAL PROCEDURE

To understand the synergistic influence of each nanofiller in the material system, six specimen groups with varying relative concentrations of MWCNTs and CCFeNPs were manufactured. All specimens were made up of an epoxy matrix modified with 0.5 wt.% of nanoparticles; either only multi-walled carbon nanotubes or only carbon-coated nanoparticles or some combination of the two that added up to 0.5 wt.%. More details about the relative filler weight fraction for each group can be found in Table 3.1. Carbon nanotubes were chosen due to their excellent electrical conductivity, high aspect ratio, and desirable tensile strength characteristics. Carbon-coated iron nanoparticles present magnetism from the iron core while the carbon coating provides an effective oxidation barrier and prevents corrosion. Hydrophilic carbon coating on iron nanoparticle cores endows better dispersibility and stability than those shown by bare iron oxide nanoparticles. This combination of electrical and magnetic fillers were selected because the complementary nature of their geometry (high aspect ratio tubes and nano-sized spheres) allows for synergistic electro-magnetic interactions in a percolated network. Epoxy was chosen as the matrix due to its widespread commercial availability and popularity.

Table 3.1. Specimen groups and their relative constituents.

Specimen group	1	2	3	4	5	6
Weight fraction of CNT (%)	0.5	0.4	0.3	0.2	0.1	0.0
Weight fraction of CCFeNP (%)	0.0	0.1	0.2	0.3	0.4	0.5

3.1 Manufacturing

Manufacturing began with weighing an appropriate amount of epoxy resin (FibreGlast System 2000). Desired quantities of MWCNTs (Cheap Tubes 30101) and CCFeNPs (Sigma Aldrich 746827) were added to the polymer for each specimen permutation. Exact dimensions of both fillers are given in Table 3.2. Surfactant (Triton X-100) was added in a 1:1 weight ratio to the nanofillers and acetone was added in a 1:1 volume ratio to the epoxy. The mixture was then stirred for 5 minutes by hand following which, it was stirred in a planetary

centrifuge mixer for the same duration. To improve homogeneity of the fillers in the polymer phase, the solution was sonicated in a tip sonicator at 50% power with pulses every other second. Two batches with different sonication times were manufactured; one sonicated for 1 hour only while the other was sonicated for 2 hours. The next step was to evaporate the diluent, which was done on a heated (60 °C) magnetic stirring (600 rpm) plate for 24 hours. Following successful removal of acetone, the solution was cooled to room temperature and an air release agent (BYK-A 501) and hardener were added. Hardener-to-epoxy ratio was set at 23:100. After stirring once again for 5 minutes, the mixture was poured into silicon molds and left to cure in an oven for 5 hours at 60 °C. A schematic describing the manufacturing process can be seen in Figure 3.1.

Table 3.2. Dimensions of nanofillers as provided by manufacturer.

Carbon nanotubes	Outer diameter: 10-20 nm
	Length: 10-30 μm
Carbon-coated iron nanoparticles	Average size: 25 nm
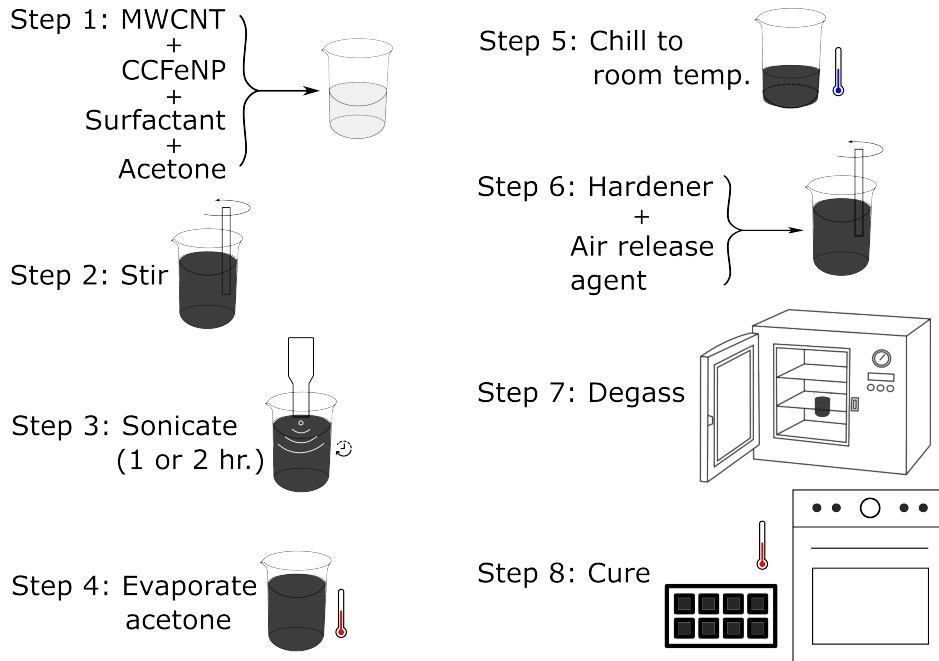
Figure 3.1. Schematic of manufacturing procedure for MWCNTs + CCFeNP/epoxy

3.2 Testing

A combination of electrical and magnetic fillers is expected to react to both electrical fields and magnetic fields. To elucidate the synergistic influence of their respective properties, a comprehensive analysis of the material was performed through electrical tests as well as magnetic tests. Thus, resistance, impedance, magnetic permeability, permittivity, and piezoresistance were measured. Each type of test equipment had a uniquely shaped specimen fixture and hence, specimens of different geometries and dimensions had to be manufactured. While electrical tests were performed on specimens sonicated for both 1 and 2 hours, all subsequent testing was done on specimens sonicated for 2 hours due to time constraints.

3.2.1 Electrical Measurements

While the electrical properties of MWCNT modified polymers have been studied considerably, it is expected that the addition of CCFeNPs would affect this performance. To gain better insight into the electrical attributes of the combined filler system, we chose to perform both DC resistance and AC impedance tests. Simple, block-like specimens were manufactured. This would provide ample surface area to prepare and mount surface electrodes on opposite faces of the specimens. This shape was chosen because of it simplicity in specimen preparation, the ease it offers to measure resistance with a simple setup, and the ability to produce multiple specimens in one manufacturing run. Opposite faces of twenty cube-like prismatic specimens from each group (each measuring 10 mm × 10 mm × 9 mm) were sanded down to expose the nanofiller network. Fast drying silver paint was applied on these faces to form surface electrodes for two-point measurements. A digital multi-meter (DMM) was used to measure the resistance across the specimens at room temperature. Figures 3.2 and 3.3 showcase representative specimens and the setup for the DC tests, respectively. Following direct current measurements, copper tape was applied to the painted faces of the same specimens to form electrode tabs. Each specimen was connected via alligator clips to an impedance analyzer (Keysight E4990A), which measured the impedance magnitude and phase angle across the specimen as a function of frequency from 20 Hz to 10 MHz. This process was repeated for 10 specimens of each group. The equivalent circuit for each specimen

was also modeled on the analyzer to quantify the resistance and reactance of the material groups. A few representative specimens and the test setup are shown in Figures 3.4 and 3.5, respectively.

Figure 3.2. Representative DC specimens. The left and ride side faces have fast drying silver paint to form surface electrodes.

3.2.2   Magnetic Measurements

To understand the effect of diamagnetic carbon nanotubes in conjunction with the ferromagnetic iron nanoparticles, bulk magnetic dipole moment m was measured as a function of applied magnetic field, H at room temperature. In this endeavor, by employing the manufacturing and casting method defined above, cylindrical specimens measuring 6.25 mm in length $\times$ 3.5 mm in diameter were manufactured for each specimen group. Figure 3.6 displays an example of these specimens. Each specimen was mounted on a cylindrical brass sample holder, the typical fixture utilized by the magnetic property measurement system (MPMS, EverCool SQUID magnetometer). The SQUID is an extremely sensitive magnetic flux-to-voltage transducer. Prior to mounting, it was ensured that each specimen was dust free. Just 4×10^{-11}g of iron is enough to produce errant noise in the measurement system of the MPMS. Only clean ceramic tools were utilized to avoid imparting magnetic impurities
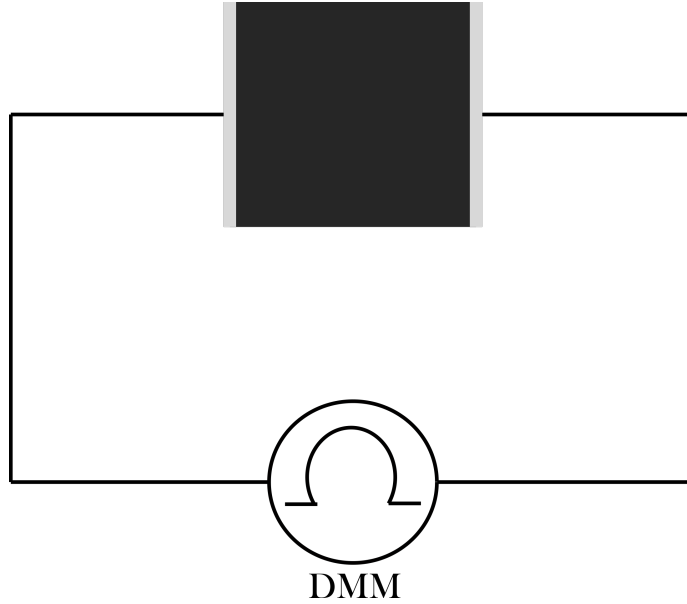
Figure 3.3. Experimental setup for DC tests.
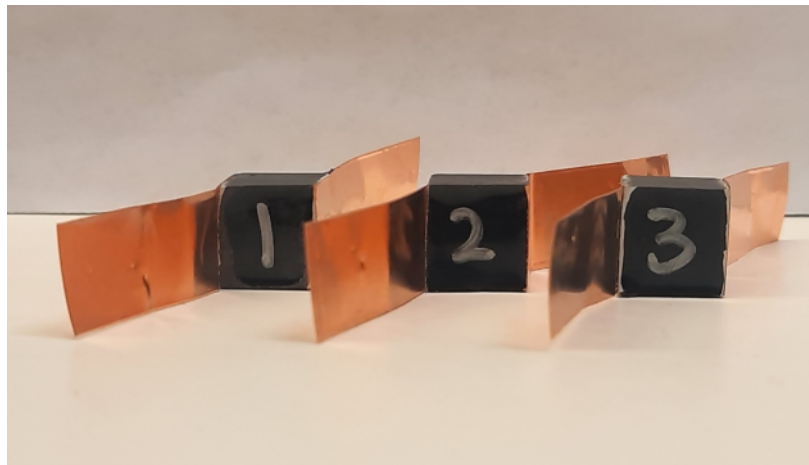
Figure 3.4. Representative AC specimens. Copper tape was applied to the left and right side faces of the DC specimens.

to the samples. After inserting the specimen, the first step was to check whether the specimen was in the center of the magnetic field. This is done by performing a centering scan. During the centering scan, the MPMS scans the entire length of the specimen and measures the offset, that is, the distance from the bottom end of the sample holder to the sample location. This is usually about 66 mm. We used the DC centering scan mode wherein the specimen moves through the detection coils and the coil response is analyzed to locate the
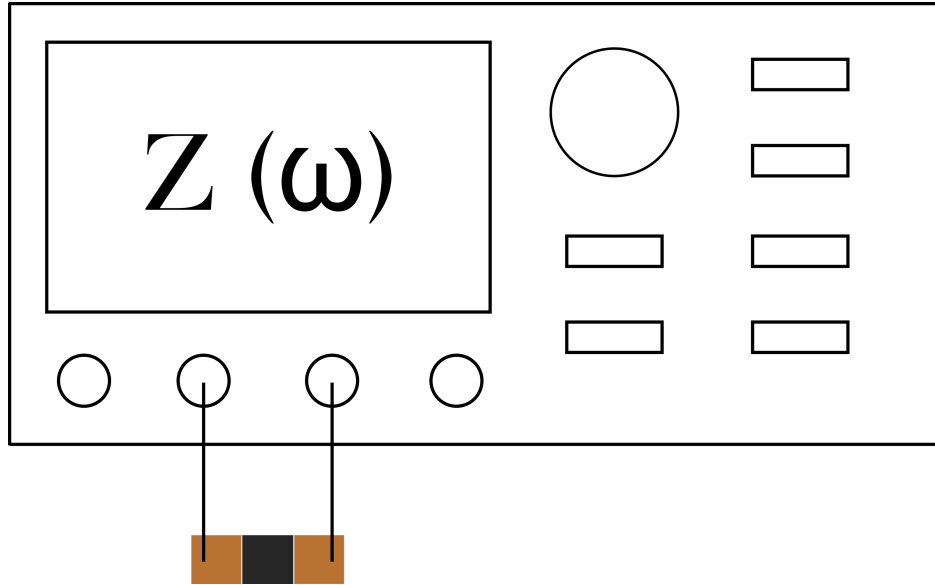
Figure 3.5. Representative equipment setup for AC tests.

specimen. Once it was ensured that the magnetic center of the specimen was within the specified tolerance (66±3 mm)[90], the vibrating sample mode (VSM) was activated and a linearly increasing magnetic field (700 Oe/s) was applied in the range of -30,000 Oe to 30,000 Oe. The resultant magnetic moment generated in three specimens was measured. Figure 3.7 showcases the respective test setup.
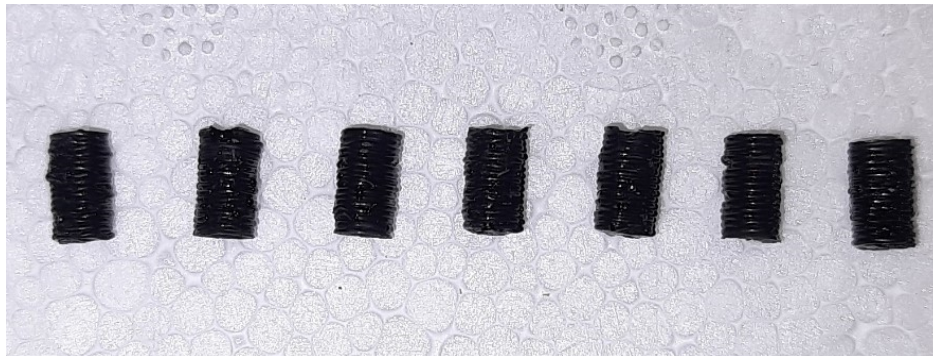
Figure 3.6. Representative magnetic specimens.
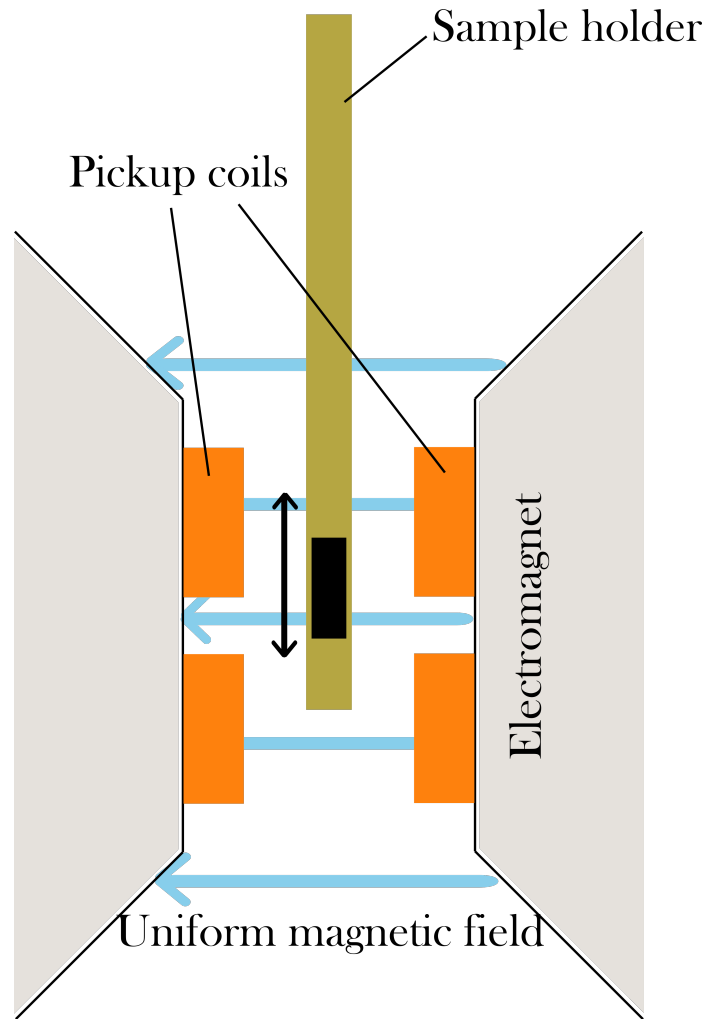
Figure 3.7. Representative test setup to measure magnetic permeability.

3.2.3 Permittivity

Permittivity was also measured for these materials per ASTM D150-81. Specimen preparation for this test began with manufacturing long cylindrical specimens (55 mm diameter $\times$ 35 mm long) in silicon molds. The non-contacting electrode method (air gap method) was employed to measure the permittivity of this material. This method derives the dielectric constant from the capacitance difference between two measurements; once without the test material, and the other with the test material. These two measurements are made with the distance between the electrodes held constant. This method eliminates the need for surface electrodes while simultaneously eliminating any errors caused by an air film (error caused

by air gap between the electrode and the surface of test material). The measurements were performed on the aforementioned impedance analyzer in conjunction with the accessory, dielectric test fixture (16451B). The accessory is furnished with four electrodes for dielectric measurements: A, B C, and D. Of the two electrodes (electrodes A and B) suitable for the air gap method, the authors chose to use electrode A for this test since it has a larger diameter. Test materials with large diameters and lower thickness yield more accurate results. The air gap method, as outlined in the 16451B user manual[91], states that when using electrode A, the diameter of the material under test should be greater than or equal to 40 mm and smaller than or equal to 56 mm. Additionally, the thickness of the test material is restricted to below 10 mm. Thus, the specimens were cut down to desired thickness (2 mm) on a horizontal band saw and cleaned with acetone. After performing rough and accurate adjustment of the guard/guarded and unguarded electrodes to ensure parallelism, the test material was set between the electrodes. The gap between guard electrode and unguarded electrode was set such that the gap distance between the guard electrode and the test material was less than 10% of thickness of the test material. The series capacitance and dissipation factor was measured as a function of frequency (20 Hz to 5 MHz). Then the material was carefully extracted from between the electrodes and the capacitance and dissipation factor was measured once again. This procedure was repeated on five specimens from each group. Figure 3.8 shows the representative specimens used in this test while Figure 3.9 shows the test setup.
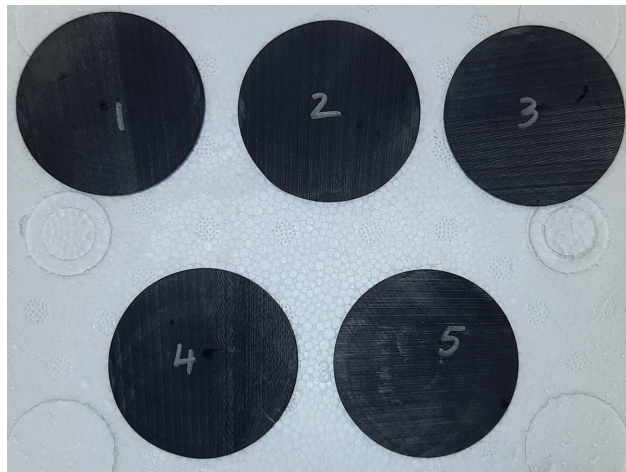
Figure 3.8. Representative permittivity specimens.
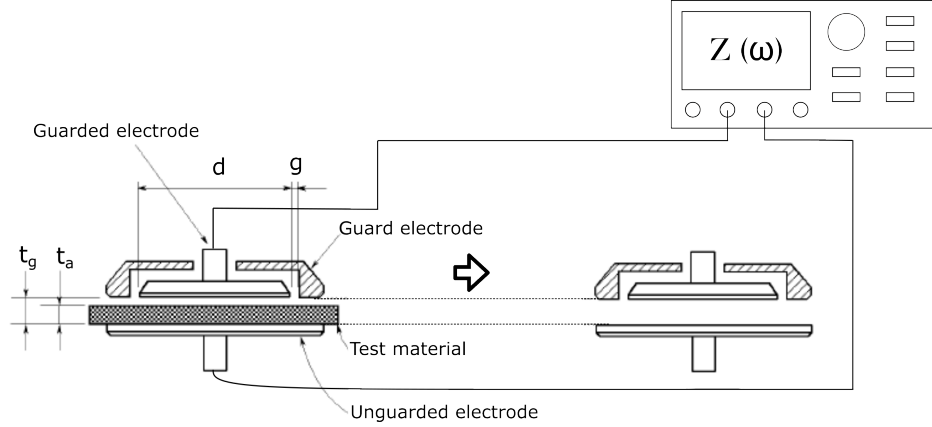
Figure 3.9. Representative test setup to measure relative dielectric constant.[91]

3.2.4 Mechanical Measurements

To understand the mechanical and piezoresistive properties of these composites, tensile testing was also conducted. For this, three dog bone shaped specimens (measuring 165.1 mm in length × 13 mm in width, gauge length 127 mm) were manufactured for each group according to ASTM D638. To establish Ohmic contact with the current supply, two 6.35 mm wide surface electrodes were prepared on the gauge section, by first sanding down the surface, applying fast drying silver paint, and then applying copper tape over the silver paint. The electrodes were positioned at a separation distance of 38.1 mm from each other. The two-point probe setup allows for easy and accurate measurement of voltage across the gauge length within the elastic range of applied strain and resistances. Grip tabs were also attached at the end of each test specimen on both the top and bottom surfaces. The specimens were mounted in the grips of a hydraulic powered load frame (Instron 8801) and electrical connection was established with a power supply via a data acquisition system (PXIe-6368 NI DAQ). An edge-mounted extensometer (2620601 Dynamic Extensometer) was employed to measure strain during the monotonically applied displacement cycle. The test method was designed to apply displacement at a rate of 0.01 mm/s for 165.1 s. This resulted in a maximum displacement amplitude corresponding to 1% engineering strain. Prior to applying mechanical load, a current-voltage sweep was conducted for each specimen to understand the conduction mechanism. After a relationship between the two was established, baseline resistance (R_0)

was measured to determine undeformed resistance. Then the test was performed, where the load frame applied tension on the specimen while the strain and voltage across the gauge section was measured. The resistance was measured after testing as well (called post experimental resistance, R_d) to determine permanent changes to resistance caused by mechanical loading. An example of the test setup can be seen in Figure 3.11.

Figure 3.10. Representative tensile specimens.
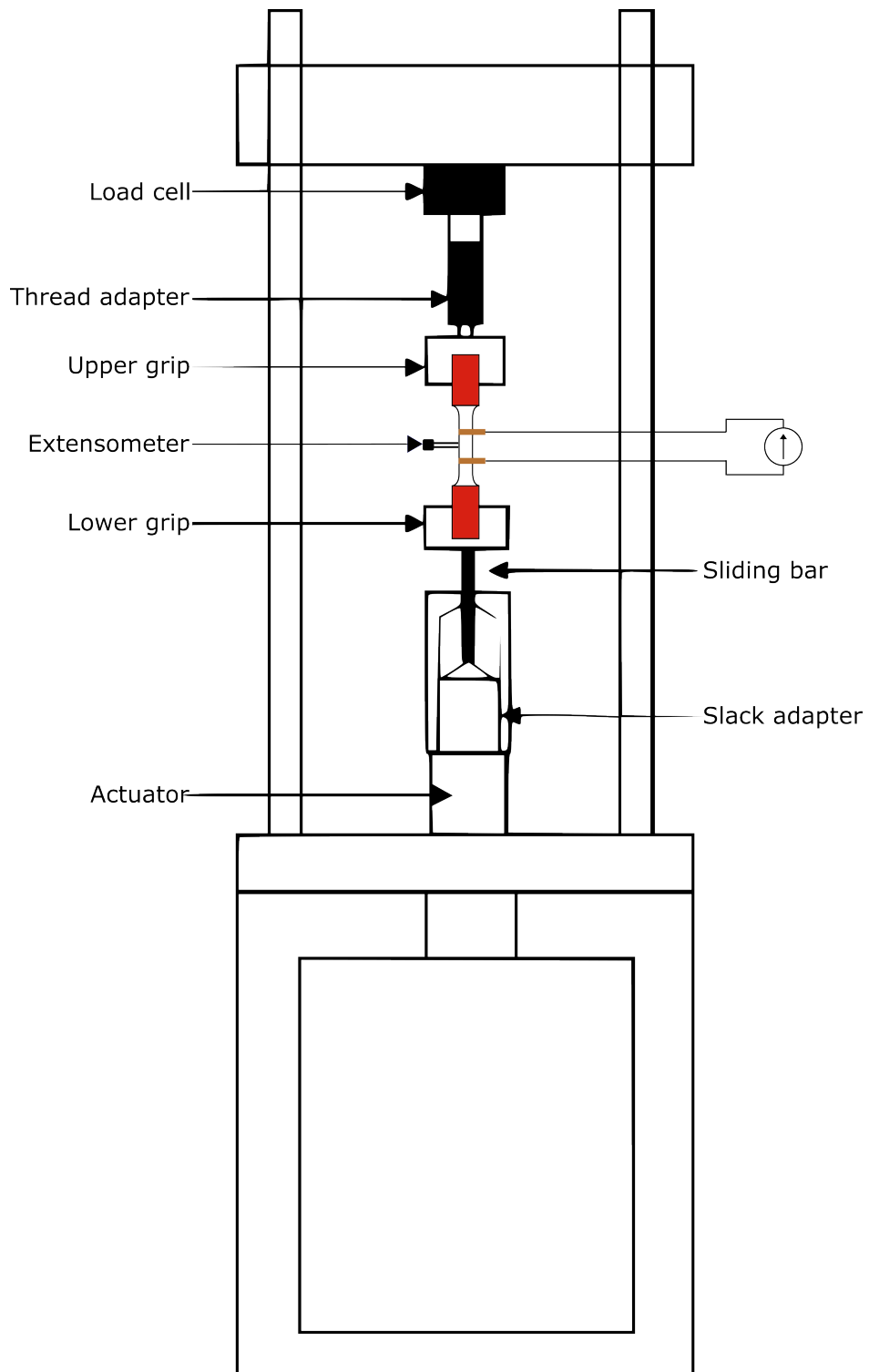
Figure 3.11. Test setup to measure strain and voltage using a two-point probe method under monotonic tensile loading.

4. EXPERIMENTAL RESULTS AND DISCUSSION

Having described the manufacturing procedure and tests deployed to characterize the material, this section details the following: original data gathered from the test equipment, data processing methods performed on the original data to determine quantities of interest, and a thorough comparison of the quantities of interest for different specimen groups. The accompanying explanation for each finding attempts to elucidate the system's behavior.

4.1 SEM Imaging

To visualize the geometry and distribution of the filler network, a few specimens from each group were frozen in liquid nitrogen and then manually fractured. The fracture surface was studied under a scanning electron microscope (Nova SEM) after applying platinum coating. Imaging shows a combination of regions with good MWCNT dispersion and regions with agglomerations of MWCNTs (see Figure 4.1). The dispersion of MWCNTs allows for a well connected conductive pathway. Under the SEM, only MWCNTs were observed whereas CCFeNP could not be seen. This could be because of their small size and low concentrations. Thus, we turned to transmission electron microscopy (TEM) on the Tecnai G2 20 for platinum coated and uncoated specimens. The uncoated specimens (see Figure 4.2) show well-dispersed CCFeNP on the observation surface. The topographical image of the composite reveals several distinct dark colored regions. CCFeNP was located in these very regions on the backscatter image. A better view of the CCFeNPs was obtained from the platinum coated specimens (see Figure 4.3). Sphere-like agglomerations of CCFeNPs can be identified on the fracture surface from the topographical image.

4.2 DC Conductivity

The average DC conductivity and standard deviation for each specimen group and different sonication times is shown in Figure 4.4. The resistivity for each specimen described in section 3.2.1 was calculated as $\rho_{DC} = AR/L$, where A is the surface area of the electrodes, R is the resistance measured across the electrodes, and L is the distance between the
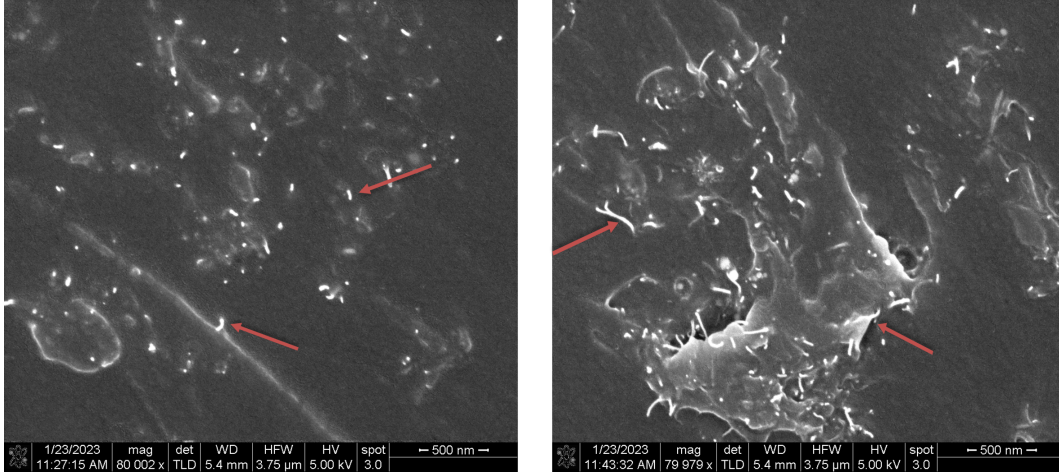
Figure 4.1. SEM images of platinum coated 0.3 wt.% MWCNT + 0.2 wt.% CCFeNP/epoxy. The left image shows MWCNTs protruding from the fracture surface (indicated by arrows) with seemingly good dispersion. The right image shows an agglomeration. CCFeNPs are unable to be definitively located in these images.

electrodes. The resulting conductivity was calculated by taking the reciprocal of this value, that is, $\sigma_{DC} = 1/\rho_{DC}$. Specimens with only CCFeNPs and no MWCNTs exhibited very high resistance and hence the resistance across these specimens was immeasurable with a DMM. This is probably attributable to the fact that the spherical CCFeNPs are present at a concentration insufficient to establish an electrically percolated network. That is, the percolation threshold of CCFeNPs in epoxy lies above 0.5 wt.%. Batches sonicated for 1 and 2 hour(s) show similar trends in DC conductivity. Specimens containing only MWCNTs have conductivity between 0.5 and 0.6 $\times 10^{-3}$ S/m. However, the addition of 0.1 wt.% CCFeNP increases the conductivity to approximately 1.1 $\times 10^{-3}$ S/m. This could be because the iron particles provide a pathway for electrical current between the carbon tubes. Similar phenomena has been documented in other multifiller composites with complementary shapes[92], [93]. With increasing relative concentration of CCFeNPs and decreasing concentration of MWCNTs, the electrical conductivity drops, as one would expect. The percolation threshold of MWC-NTs lies between 0.2 and 0.3 wt.% and thus very low values of conductivity are recorded for 0.3 wt.% MWCNT + 0.2 wt.% CCFeNP/epoxy and 0.2 wt.% MWCNT + 0.3 % CCFeN-P/epoxy. One prominent difference caused by longer sonication times can be noticed in the
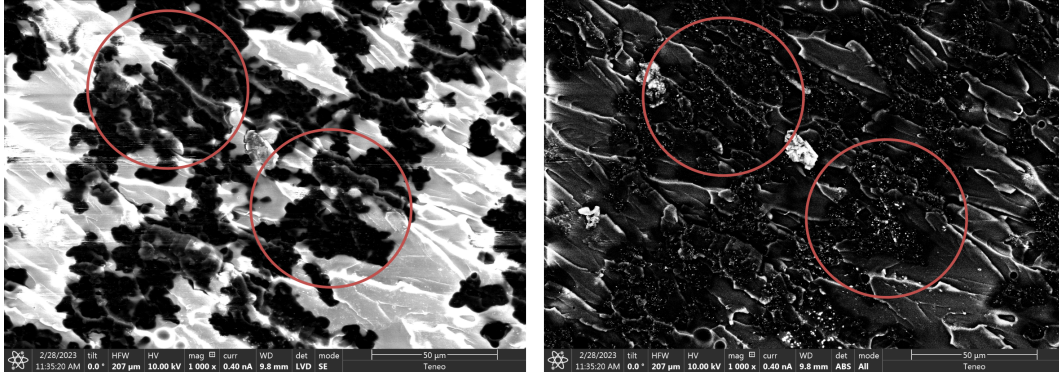
Figure 4.2. TEM images of uncoated 0.5 wt.% MWCNT + 1 wt.% CCFeN-P/epoxy. On the left is a topographical image of the fracture surface while the right is a backscatter image of the same. The backscatter image indicates that CCFeNP is well dispersed. The encircled regions on the right correspond to where CCFeNP is located. The illuminated areas in the encircled regions on the right indicate the presence of CCFeNP. These regions appear as dark colored patches on the left.
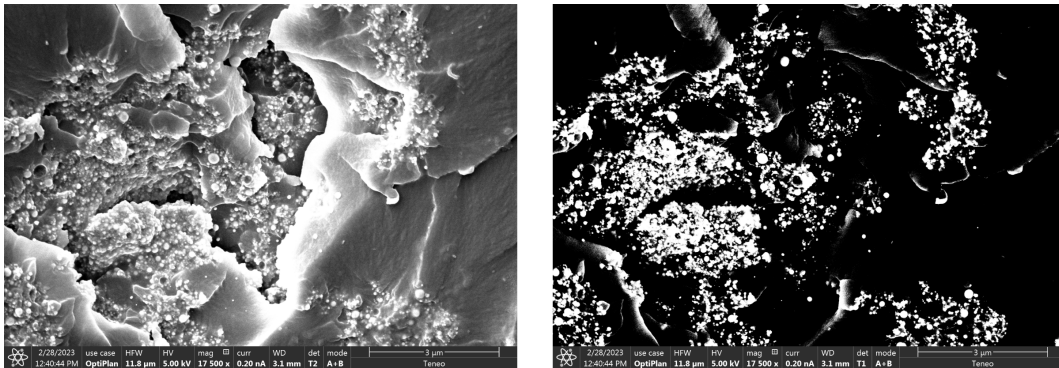
Figure 4.3. TEM images of platinum coated 0.5 wt.% CCFeNP/epoxy. On the left is a topographical image of the fracture surface while the right is a backscatter image of the same. These images show an agglomeration of iron particles.

electrical response of the 0.1 wt.% MWCNT + 0.4 wt.% CCFeNP group. The reason for this dramatic difference in electrical conductivity with sonication times is currently unknown. However, it can be hypothesized that longer sonication introduces the risk of damaging the MWCNTs, thereby decreasing their aspect ratio. And since aspect ratio is closely tied to conductivity[94], it may cause the significant change in conductivity seen here (almost 75%).
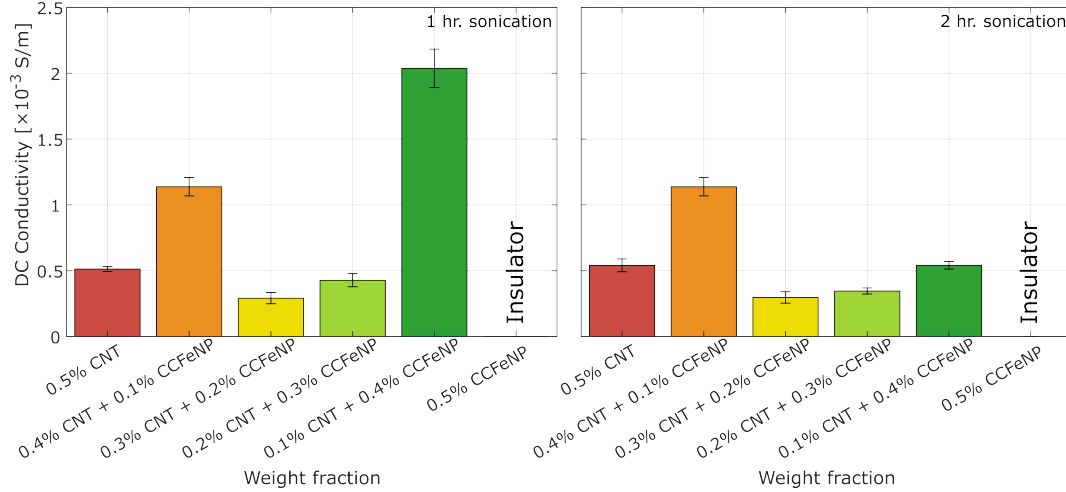
Figure 4.4. Average DC conductivity for each relative weight fraction and two sonication times. The dashes indicate the standard deviation of twenty specimens from each group.

4.3 AC Conductivity

The average AC conductivity for each group was determined from the measured impedance magnitude and phase angle (shown in Figures 4.5 and 4.6). Electrical impedance spectroscopy (EIS) curves shown in Figure 4.9 were generated from the impedance magnitude and phase angle by using equations 4.1 and 4.2 where $|Z|$ and θ are the impedance magnitude and phase angle. The real part of impedance is called resistance while the imaginary part of impedance is called reactance. Note, however, that 'resistance' is just a nomenclature term; the real part of the impedance can also include non-resistive transport mechanisms. Similar to the DC measurements, CCFeNP only specimens were non-conductive and therefore are excluded from these results. Each point on the EIS curve is the impedance at one value of frequency. The EIS plots show a semi-circular trend, indicating that the material exhibits behavior typically seen in parallel resistor-capacitor circuits. However, specimens with 0.3 wt.% MWCNT + 0.2 wt.% CCFeNP in the first batch and 0.4 wt.% MWCNT + 0.1 wt.% CCFeNP in the second batch show very large standard deviations. The real impedance and reactance were plotted as a function of frequency (shown in Figures 4.7 and 4.8). For longer sonication (right figure), the addition of CCFeNPs to MWCNTs, that is, 0.4 wt.% MWCNT + 0.1 wt.% CCFeNP/epoxy shows both high reactance and high real impedance. Similar

behavior is observed for the 0.3 wt.% MWCNT + 0.2 wt.% CCFeNP/epoxy group in the first batch (left figure). It is possible that the increased interfacial zones between nanofillers leads to greater resistive losses[95]. When two conductive particles are held at close proximity and the separation distance is occupied by an insulating material (for example, epoxy), a capacitor is made. At the micro scale, when one has large quantities of nanoscale conductive particles suspended in epoxy, one can expect at least some of them to behave like micro-capacitors. If we assume that the MWCNTs and CCFeNPs are dispersed well enough to behave like micro-capacitors, this could explain the high reactance we observed.

$$Re(Z) = Z' = |Z|\cos(\theta) \tag{4.1}$$

$$Im(Z) = Z'' = |Z|\sin(\theta) \tag{4.2}$$
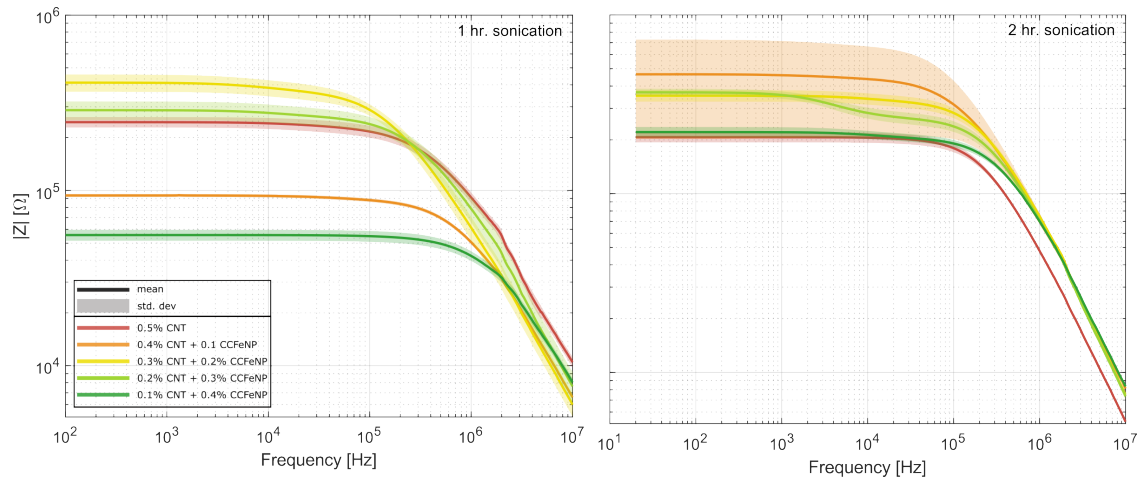
Figure 4.5. Impedance magnitude as a function of frequency for all specimen groups and two sonication times on a log plot. The solid lines indicate the mean of ten specimens from each group and the shaded regions indicate the standard deviation.

The test equipment also curve-fitted the impedance magnitude and phase angle to the response of standard resistor-inductor-capacitor circuits. The electrical response of almost all specimens curve-fitted well to the electrical characteristics of the circuit shown in Figure 4.10. The average curve-fitted values of resistance, inductance, and capacitance are shown in
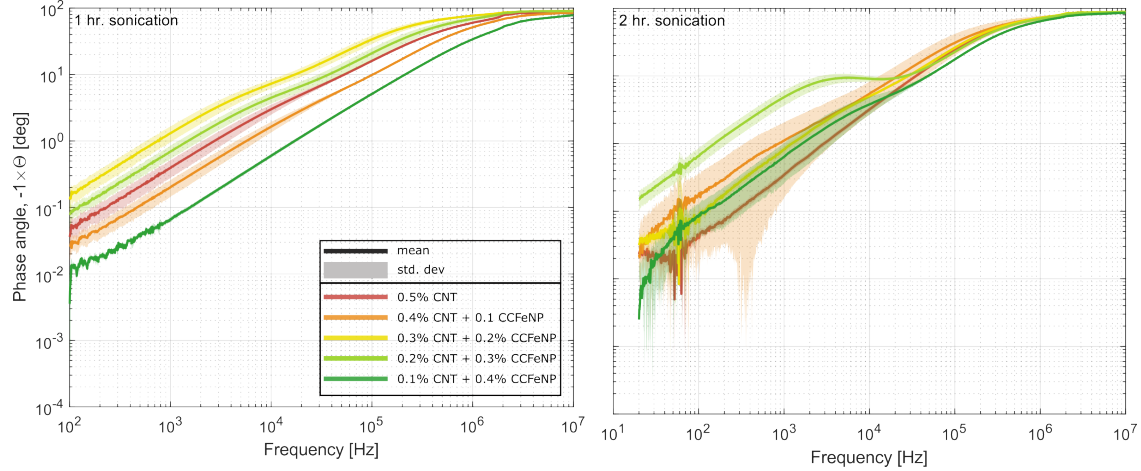
Figure 4.6. Phase angle as a function of frequency for all specimen groups and two sonication times on a log plot. The solid lines indicate the mean of ten specimens from each group and the shaded regions indicate the standard deviation.

Figure 4.11. If one assumes the behavior of the material to be similar to the behavior of the circuit shown in Figure 4.10, the following conclusions can be made. Results from the first batch show that the 0.1 wt.% MWCNT + 0.4 wt.% CCFeNP group has the lowest resistance but significant inductance and capacitance. This could mean that the iron particles have good electrical contact. Similarly, the 0.4 wt.% MWCNT + 0.1 wt.% CCFeNP specimen group showed low resistance but considerable capacitance, indicating that the conductive tubes are in such close proximity that they are behaving like micro-capacitors. On the other hand, the same specimen group when sonicated for longer exhibits very high resistance. It is possible that the longer sonication may have resulted in better dispersion of MWCNTs. This would increase the interfiller distance between MWCNTs in the system which could lead to a higher resistance.

For prismatic specimens discussed in section 3.2.1, the AC conductivity can be calculated as $\sigma_{AC} = L/Z'A$ where L is the length between the electrodes, Z' is the real part of impedance (refer to equation 4.1), and A is the area of the electrodes. Average AC conductivity versus frequency is shown in Figure 4.12. The AC conductivity shows two distinct regimes; frequency-independent behavior (the flat part of the curves, also called the DC region) and frequency-dependent behavior (where the curves grow exponentially). In the DC
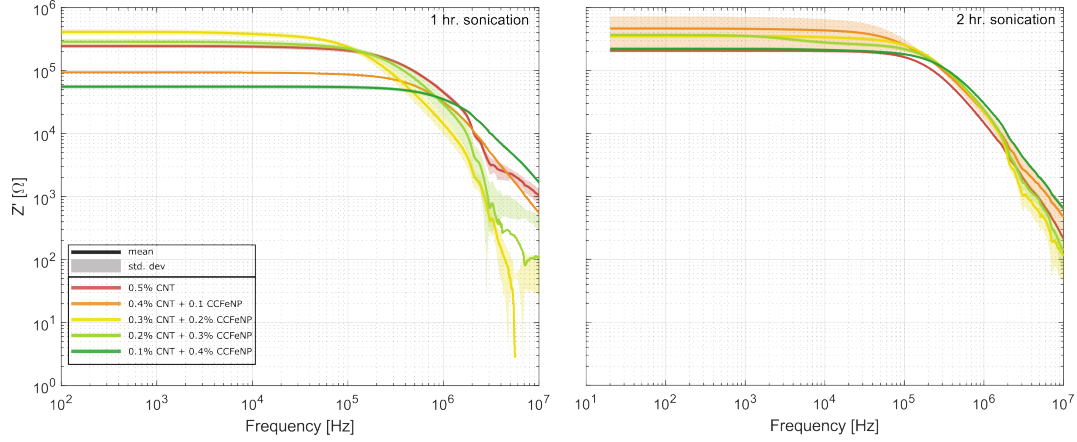
Figure 4.7. Real impedance as a function of frequency for all specimen groups and two sonication times on a log plot. The solid lines indicate the mean of ten specimens from each group and the shaded regions indicate the standard deviation.
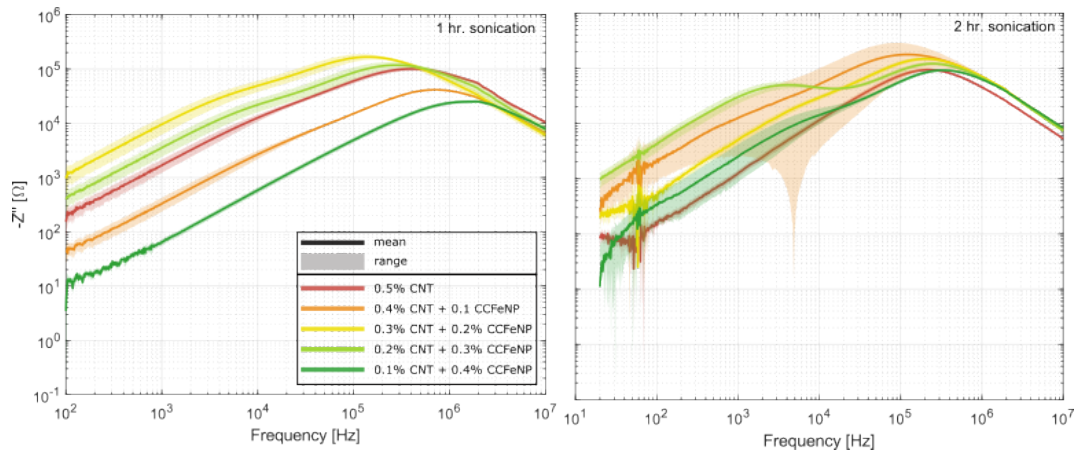
Figure 4.8. Reactance as a function of frequency for all specimen groups and two sonication times on a log plot. The solid lines indicate the mean of ten specimens from each group and the shaded regions indicate the standard deviation.

region, electrical behavior is controlled by filler and inter-filler resistance only. However, in the frequency-dependent region, the frequency is high enough for the impedance to be impacted by frequency-dependent effects such as inter-facial polarization between conductive fillers and insulating matrix, inter-filler regions behaving like micro-capacitors, etc. Both batches display noisy behavior above 1 MHz, although it is to a much greater extent for the first batch (1 hour sonication). This could be because longer sonication allows for better
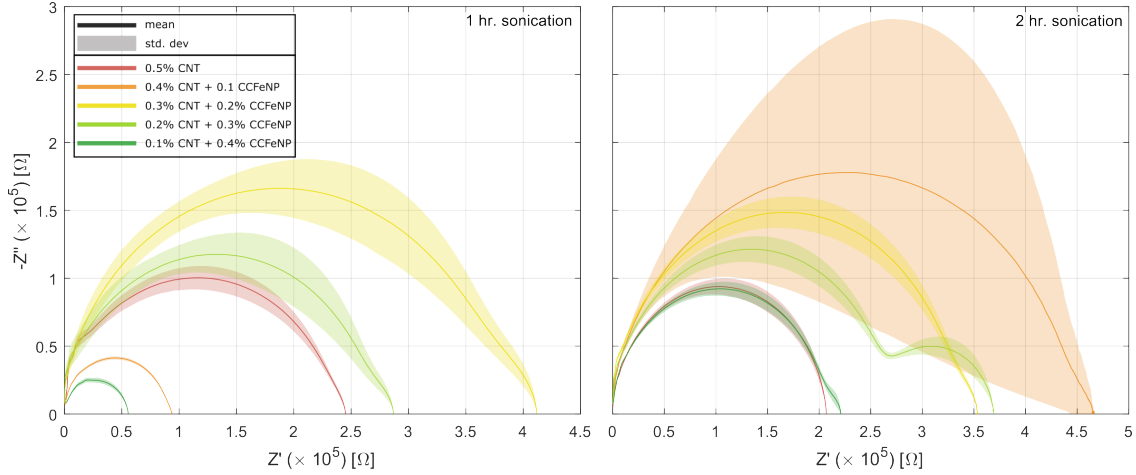
Figure 4.9. EIS curves for each relative weight fraction and two sonication times. The solid lines indicate the mean behavior of ten specimens while the shaded regions indicate the standard deviation.
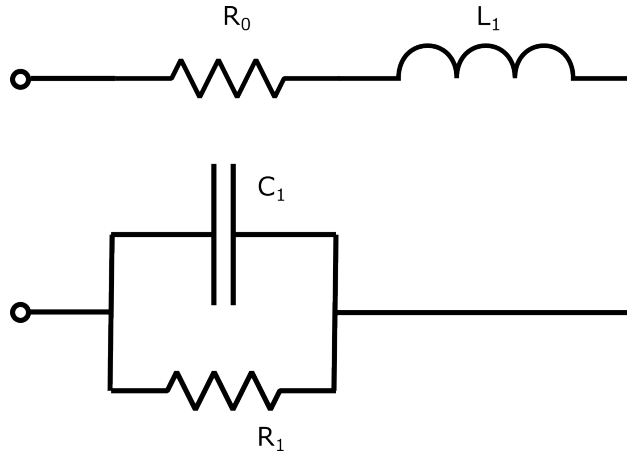
Figure 4.10. RLC circuit curve-fitted to the measured data for all specimen groups and batches.

dispersion of the fillers in the epoxy matrix. And better dispersion translates to a well established electrical network. For the first batch, specimens containing 0.1 wt.% MWCNT + 0.4 wt.% CCFeNP show highest AC conductivity in the frequency range 100 Hz to 0.1 MHz, about 2×10^{-3} S/m. This is followed by the 0.4 wt.% MWCNT + 0.1 wt.% CCFeNP group. Similar trends were observed in DC conductivity as well. However, for the second batch, at sub-MHz frequencies, MWCNT-only specimens show the highest conductivity at 5.6×10^{-3} S/m, which is followed closely by 0.1 wt.% MWCNT + 0.4 wt.% CCFeNP. The 0.4 wt.%
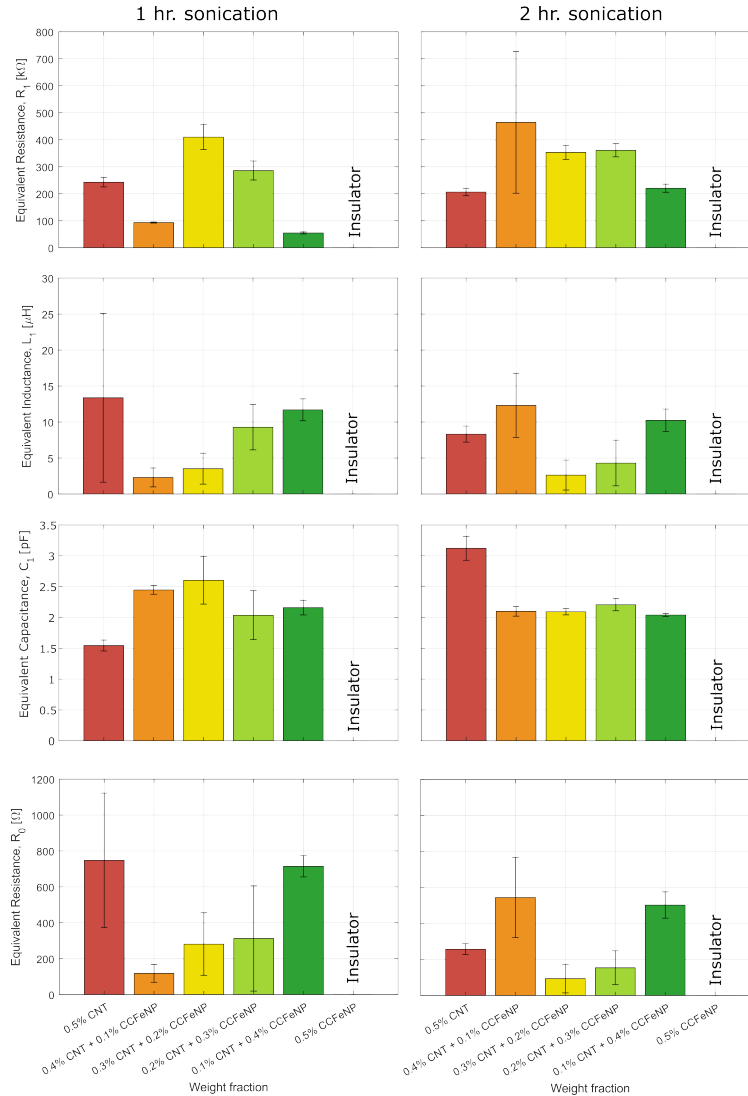
Figure 4.11. Average curve-fitted values of resistance, inductance, and capacitance for each specimen group and two sonication times. The dashes indicate standard deviation of ten specimens.

MWCNT + 0.1 wt. % CCFeNP specimen group displays lowest AC conductivity, which is in direct contrast to what was seen in DC conductivity. Previous work in multifiller composites has shown that the conductivity of metal/MWCNT/polymer composites is related to many factors, such as the intrinsic conductivity of MWCNT, the length to diameter ratio of MWCNTs, the intrinsic conductivity of metal particles, the size of metal particles, the coverage ratio of metal particles, the metals work function, and the polymers work function[96].
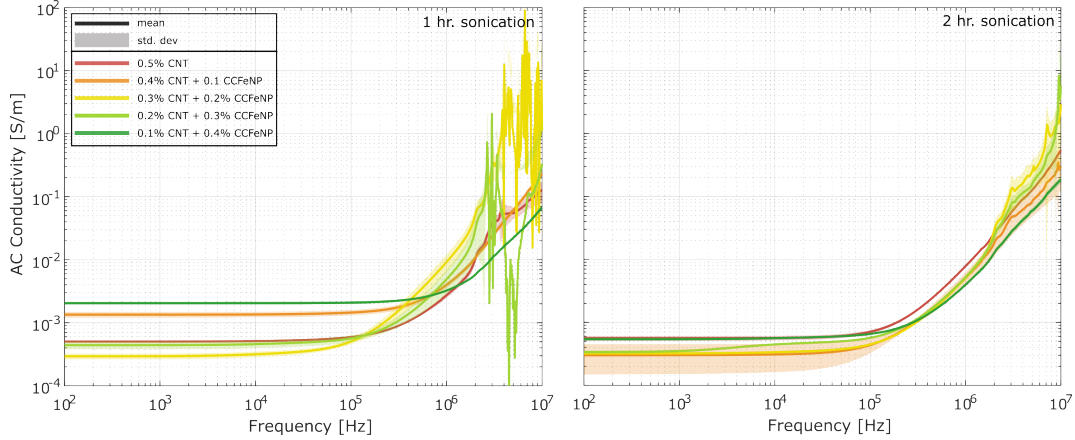
Figure 4.12. AC conductivity as a function of frequency for each relative weight fraction and two sonication times on a log plot. The solid lines indicate the mean behavior of ten specimens and the shaded regions indicate the standard deviation.

4.4 Permeability

Permeability characterizes the interaction of a material with a magnetic field. After collecting raw data (applied magnetic field and resultant bulk magnetic dipole moment m), we first corrected for magnetic remanence. Remanence or residual magnetization is the magnetization left behind in ferromagnetic material after an external magnetic field is removed. This effect becomes more pronounced at lower values of applied magnetic fields (< 1 T). The SQUID is equipped with a superconducting magnet which exhibits magnetic polarization at low fields because of pinned magnetic flux lines. The effect of magnetic remanence at low fields is an offset error in the reported magnetic field. This offset depends on the magnet history and is opposite in sign when coming from positive versus negative fields. For our purposes, the test script was designed to obtain field accuracy within 1 Oe. Next we corrected for demagnetization effects. This is a magneto static effect which creates a difference in the internal field generated in the specimen and the applied field. In cgs units, this is expressed by equation 4.3, where H is the applied field in Oe, M is the magnetic moment per unit volume in emu/cm^3 and N is the demagnetizing factor. According to the work by D-X Chen et al.[97], $N = 0.2186$ for cylinders with a length to diameter ratio of 1.6.

$$H_{in} = H_{applied} - 4\Pi NM \qquad (4.3)$$

After correcting the applied field, we had to correct the magnetic moment. The SQUID is calibrated on a palladium cylinder (measuring 2.8 mm in diameter × 3.8 mm in height). Since our specimens did not match the calibrated standard, the reported moment had an inherent error. We have to account for a multiplicative artifact (also called moment artifact) which is geometry dependent. It is determined by a simulator program and usually varies between 5-20% of the original sample dimensions. The corrected moment was determined as correct moment [emu] = reported moment [emu]/moment artifact. Cylindrical specimens present the possibility of radial and axial positioning errors. A sample that is axially out of center will lead to an under-reported moment while a sample radially out of center will lead to an over-reported moment. The simulator program allows for a radial offset. The radial offset is more crucial and can lead to 10-20% over-reported moment if the sample is not mounted carefully. A quartz paddle sample holder can be employed to minimize radial error. The corrected magnetic moment per unit volume, or magnetization experienced by the composites was determined as a function of externally applied magnetic field strength for three specimens of each weight fraction combination. Due to the small size and low weight fraction of magnetic fillers, each specimen contains approximately 0.3 mg or less of iron nanoparticles. Thus, the magnetization is not much larger than the applied field. Average magnetization, saturation magnetization and the range of magnetization for each specimen group are shown in Figure 4.13. Since carbon is diamagnetic, no measurable response was recorded for 0.5 wt.% MWCNT/epoxy. It can be observed that with increasing concentration of CCFeNPs, the saturation magnetization generally increases (also see Figure 4.14, left), which is to be expected since saturation magnetization is directly proportional to the quantity of iron. The saturation magnetization (M_{sat}) represents the maximum magnetic moment per unit volume for a magnetic material. The mean of this value drops between specimens with 0.4 wt.% CCFeNP and 0.5 wt.% CCFeNP by 1.66×10^{-4} emu/cm^3. This trend is a significant deviation from the trends observed in bulk magnetic materials. One factor that determines the saturation magnetization of a material is the magnitude of the

atomic magnetic moments[98]. Thus, one would expect that higher concentrations of iron in the composite would produce a larger magnitude of magnetic moments. However, the addition of 0.1 wt.% carbon trumps the addition of 0.1 wt.% iron when it comes to saturation magnetization. It can be hypothesized that the magnetized ferromagnetic particles induce contact magnetism in the carbon tubes due to charge transfer at the points of contact, as seen in the work by Cespedes et al.[99].
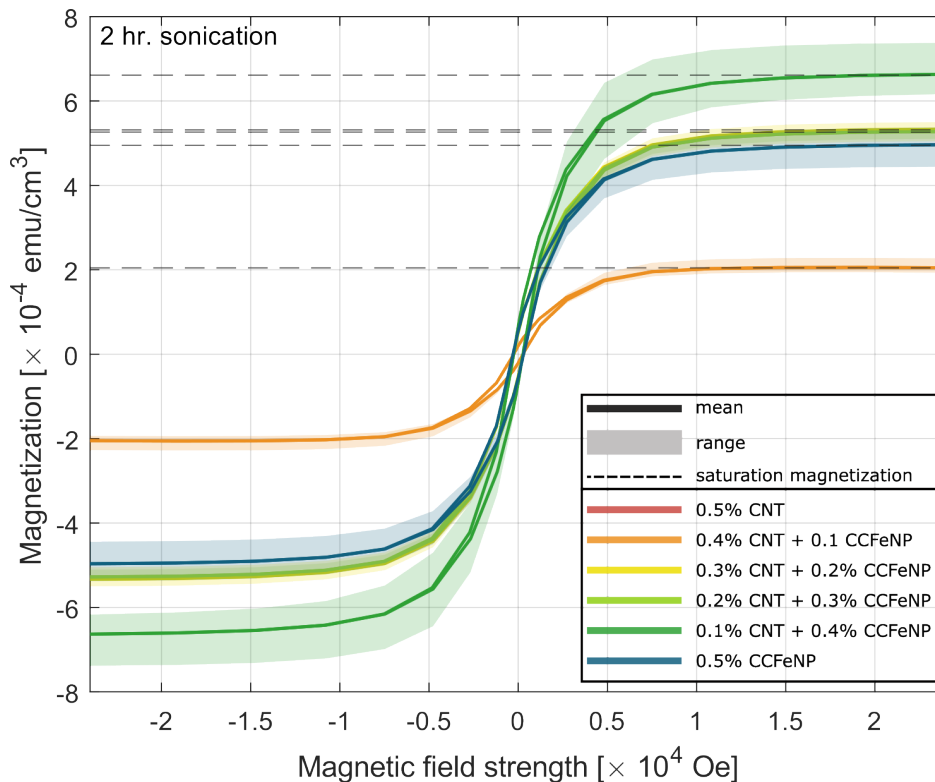
Figure 4.13. Average magnetization versus magnetic field strength for each relative weight fraction. The solid lines indicate the mean behavior of three specimens from each group, the shaded regions indicate the range and the dashed lines indicate the saturation magnetization.

Magnetic susceptibility was also determined as $\chi = M/H$, where M is the magnetization in emu/cm^3 and H is the applied magnetic field in Oe. Susceptibility is a measure of the degree to which a material can be magnetized in the presence of a magnetic field. Most materials respond with either an alignment of polar dipoles along the direction of the field, called paramagnetism ($\chi > 0$) or an alignment against the field, called diamagnetism ($\chi < 0$). It indicates whether the material system is attracted by or repelled out of a magnetic field.
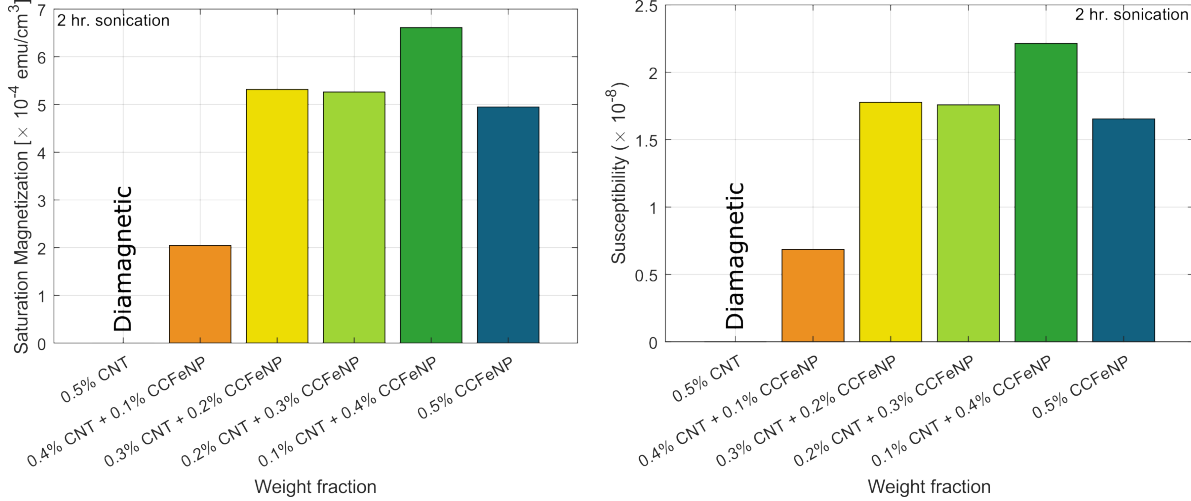
Figure 4.14. Average saturation magnetization (left) and susceptibility (right) for each relative weight fraction. Since carbon is diamagnetic, no response was recorded for 0.5 wt.% MWCNT.

The average susceptibility is presented in Figure 4.14(right). MWCNT-only specimens are diamagnetic and therefore exhibit a small negative susceptibility. The measured value of susceptibility for CCFeNP-only specimens deviates from bulk values. This could be attributed to many factors, like geometry, surface effects in these nano-scale particles, or the presence of a diamagnetic matrix[100]. The average coercivity and retentivity are also shown in Figure 4.15. These values were determined from the hysteresis loops in Figure 4.13. Coercivity is a measure of the ability of a ferromagnetic material to withstand an external magnetic field without becoming demagnetized while retentivity is the tendency of the magnetic material to retain magnetism, even in the absence of a magnetizing field. Susceptibility and retentivity are expected to rise with increasing quantities of magnetic material in the specimens, which is what we observe. However, the addition of MWCNTs enhances both these properties greater than that of CCFeNP-only specimens. More work is needed to determine if these observations regarding the change from 0.4 to 0.5 wt.% CCFeNP are due to the inclusion of the MWCNTs (i.e., a synergistic effect) or are within experimental error. And as one would expect, the coercivity of 0.5 wt.% CCFeNP/epoxy is highest since it contains the maximum amount of ferromagnetic particles.
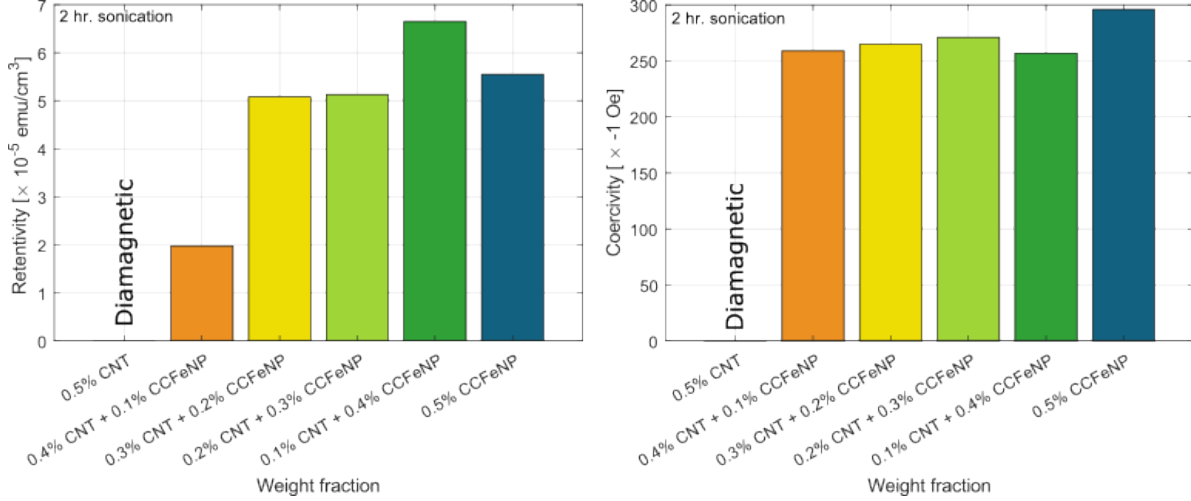
Figure 4.15. Average retentivity (left) and coercivity (right) for each relative weight fraction. Since carbon is diamagnetic, no response was recorded for 0.5 wt.% MWCNT.

4.5 Permittivity

The dielectric constant is the ratio of permittivity of the material to the permittivity of vacuum. This is also called the relative permittivity of a material which possesses the ability to collect and store energy in the form of electrical charge. Permittivity, on the other hand, is the ability of a material to store electrical energy in the presence of an electric field. Dielectric constant (κ) of a material is equivalent to its relative permittivity (ε_r)[101]. The real part of permittivity (ε_r') measures the amount of energy stored in the material from an external electric field. The imaginary part of permittivity (ε_r'') is called the loss factor and indicates how dissipative a material is to the external field. The latter is always greater than zero and usually much smaller than the former. Dissipation is usually a combination of dielectric loss as well as conductive current.

To characterize this material system, we determined the relative dielectric constant and dissipation factor, using equations 4.4 and 4.5, for each specimen group. Here C_{s1} is capacitance without test material inserted (measured in F), D_1 is the dissipation factor without test material inserted, t_g is the gap between guard/guarded electrode and unguarded electrode (in m), C_{s2} is the capacitance with the test material inserted (measured in F), D_2 is the dissipation factor with the test material inserted, t_a is the average thickness of the test

material (in m), ε_r is the dielectric constant of the test material, and D_t is the dissipation factor of the test material. C_{s1}, D_1, C_{s2}, and D_2 were measured on the impedance analyzer while t_g and t_a were set on the micrometer connected to the electrodes.

$$\varepsilon_r = \frac{1}{1 - (1 - \frac{C_{s1}}{C_s2}) \times \frac{t_g}{t_a}} \tag{4.4}$$

$$D_t = D_2 + \varepsilon_r \times (D_2 - D_1) \times (\frac{t_g}{t_a} - 1) \tag{4.5}$$

The dielectric constant of a material is a measure of its ability to store electrical energy. It is an expression of the extent to which a material holds or concentrates electric flux. The results for average relative dielectric constant and dissipation factor are shown in Figures 4.16 and 4.17. All permutations had one common trend; the value of ε_r gradually decreased with increasing frequency before plateauing at a constant value. Frequency dependence arises because of three effects: the dispersion of MWCNTs in the polymer, the polarizability between distinct MWCNT aggregates, and spatial heterogeneity within filler aggregates[102]. For heterogeneous polymers, there exists electronic, atomic, orientation, and interfacial polarization. In the presence of an alternating electric field, free charge moves inside filler clusters in the direction of applied field for each half of the current cycle. Charges accumulate on the interfacial boundaries between MWCNTs aggregates and epoxy, and a dipole moment is imparted to the cluster. It is possible that with increasing frequency, the polarization of the interfacial dipoles was weakened. This phenomenon has been documented previously as well[48]. It can be observed that the 0.3 wt.% MWCNT + 0.2 wt.% CCFeNP group has the highest relative dielectric constant in the domain of interest. This is followed by 0.5 wt.% MWCNT/epoxy and 0.2 wt.% MWCNT + 0.3 wt.% CCFeNP/epoxy. As mentioned previously, the percolation threshold of MWCNTs is between 0.2 wt.% and 0.3 wt.%. Consequently, when the composite contains quantities of carbon near this value the relative dielectric constant could increase by several orders of magnitude, according to the polarization theory by Maxwell-Wagner-Sillers[103]. On the other hand, the polarizability of composites also increases with increasing concentrations of electrical fillers because interfacial area between MWCNTs and the matrix increases simultaneously[104]. The high

aspect ratio of MWCNTs could dominate the polarizability, thereby rendering the material with good dielectric properties.
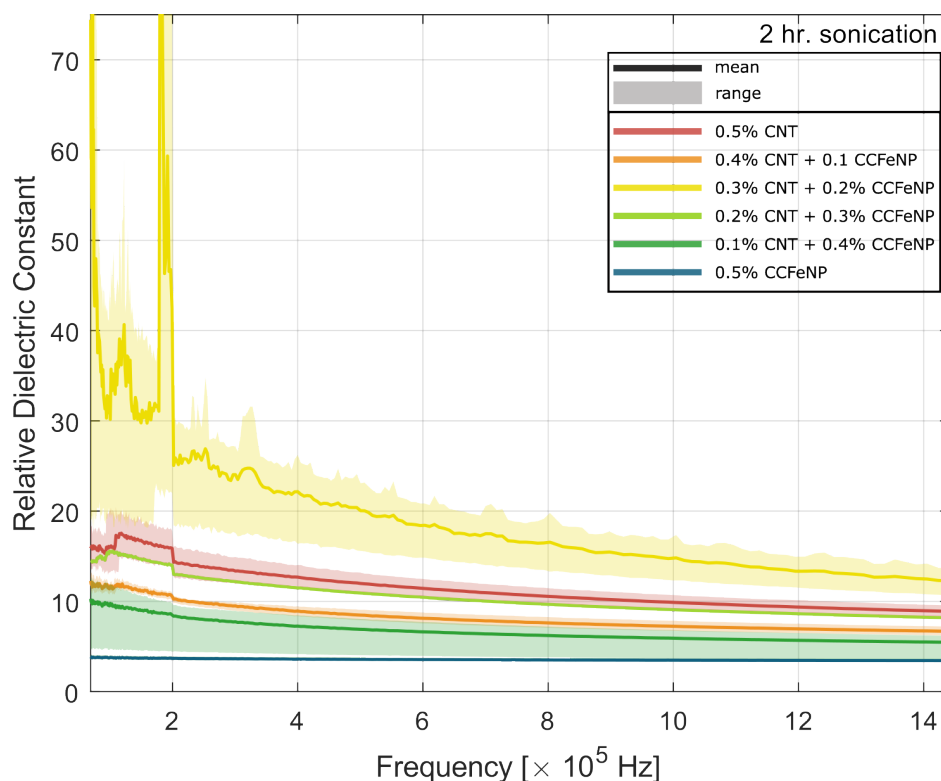
Figure 4.16. Average relative dielectric constant as a function of frequency for each relative weight fraction. The solid lines indicate the mean behavior of five specimens while the shaded regions indicate the range of measured values.

A dielectric material usually has low electrical conductivity but can store an electrical charge. When it is placed in an electrical field, no electric current flows within it. This is because the material does not have loosely bound (free) electrons that drift through it. Specimens with the lowest electrical conductivity (0.3 wt.% MWCNT + 0.2 wt.% CCFeNP, (see Figure 4.4) exhibit the highest dielectric constant. Therefore, it is possible that even though these specimens have a low concentration of free charge carriers, the filler network stores electrical energy well.

Dissipation factor is defined as the reciprocal of the ratio between a material's capacitive reactance to its resistance. Similar to dielectric constant this quantity is also frequency dependent. As the frequency increases, more energy is lost due to rapid switching of dipoles.
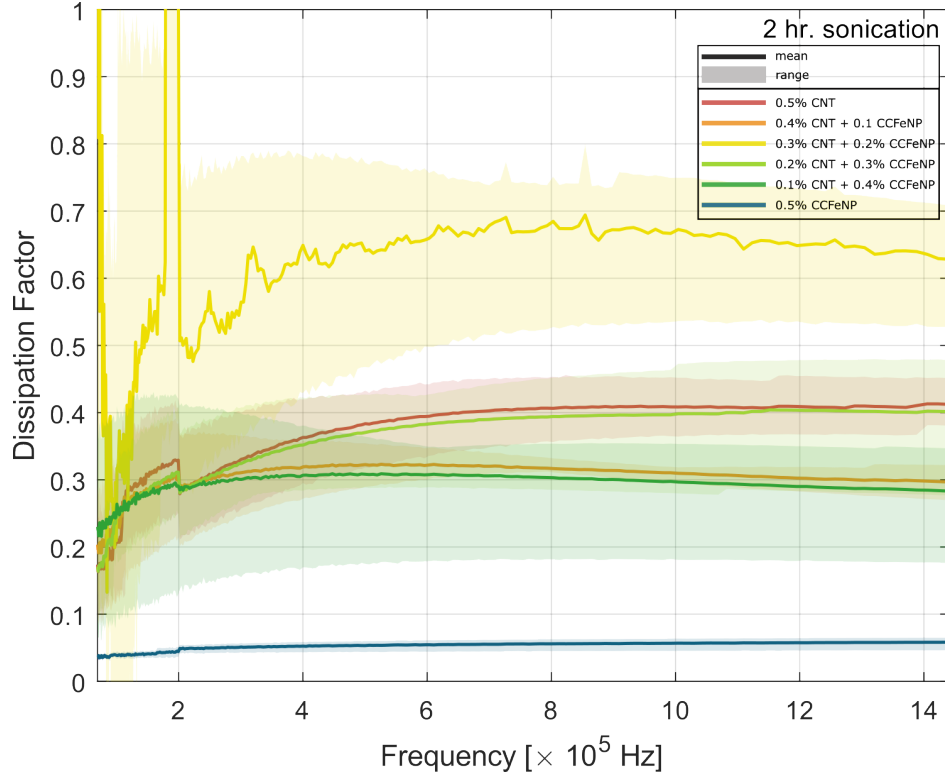
Figure 4.17. Average dissipation factor as a function of frequency for each relative weight fraction. The solid lines indicate the mean behavior of five specimens while the shaded regions indicate range of measured values.

Specimens with 0.3 wt.% MWCNT + 0.2 wt.% CCFeNP have the highest dissipation factor. The conductive path formed by MWCNTs allows a portion of the electrical energy to be lost as heat. It is possible that the addition of iron to the material adds interfacial zones which facilitates charge transfer in the material. It could lead to an increased energy loss by the free charges through the interfacial regions of the MWCNTs and CCFeNPs[105]. There exists a possibility of measurement error in this test. The causes of these errors and steps to mitigate them are listed in Appendix A.

4.6   Piezoresistance

The results of the current-voltage sweeps described in section 3.2.4 are shown in Figure 4.18. It represents the average normalised I-V curves for each specimen group as a scatter plot. The baseline resistance for each specimen was different, and hence the current-voltage

Table 4.1. Average baseline resistance, post-experimental resistance, and change in resistance for each specimen group.

Specimen group	Baseline resistance ($R_0, [M\Omega]$)	Post-experimental resistance ($R_d, [M\Omega]$)	Change in resistance ($\Delta R, [k\Omega]$)
0.5 wt.% MWCNT	2.0621	2.0802	18.11
0.4 wt.% MWCNT + 0.1 wt.% CCFeNP	49.268	49.636	367.6
0.3 wt.% MWCNT + 0.2 wt.% CCFeNP	50.07	50.201	131.43
0.2 wt.% MWCNT + 0.4 wt.% CCFeNP	203.25	203.55	305.67
0.1 wt.% MWCNT + 0.4 wt.% CCFeNP	184.7	185.45	747.52
0.5 wt.% CCFeNP	203.68	203.75	78.731

curves were normalized to aid the direct comparison of different specimen groups. To determine whether the behavior was Ohmic or not, the I-V response was compared against that of a perfect Ohmic resistor (resistance is constant). A perfect Ohmic resistor is expected to show a linear relationship between normalized current and voltage, as shown by the black line. We can observe that specimens containing none or low quantities of MWCNTs, that is, 0.5 wt. %CCFeNP/epoxy and 0.1 wt.% MWCNT + 0.4 wt.% CCFeNP/epoxy, show a slight deviation from the linear fit. This could be associated with the percolation threshold of MWCNTs. At less than 0.2 wt.%, the amount of MWCNTs is insufficient to establish a good conductive network. Thus, the relationship between current and voltage is influenced by other factors like capacitance and inductance. The non-linearity of the I-V curves vanishes for specimens with 0.3 wt.% or higher concentration of MWCNTs. The average baseline resistance (R_0), post-experimental resistance (R_d) and the change between the two (ΔR) can be found in Table 4.1. The largest change in resistance is observed in the 0.1 wt.% MWCNT + 0.4 wt.% CCFeNP specimen group. This could be attributed to the low concentration of MWCNTs. The amount of MWCNTs in this group is lower than the percolation of MWCNTs and thus permanent distortion of the electrical network would be expected to produce the largest change in material resistivity.

During mechanical testing, two quantities were measured as a function of time; engineering strain (ϵ) and voltage across the specimens for a fixed current. The dimensions of the specimens were known and hence, the applied axial stress was determined as a function of
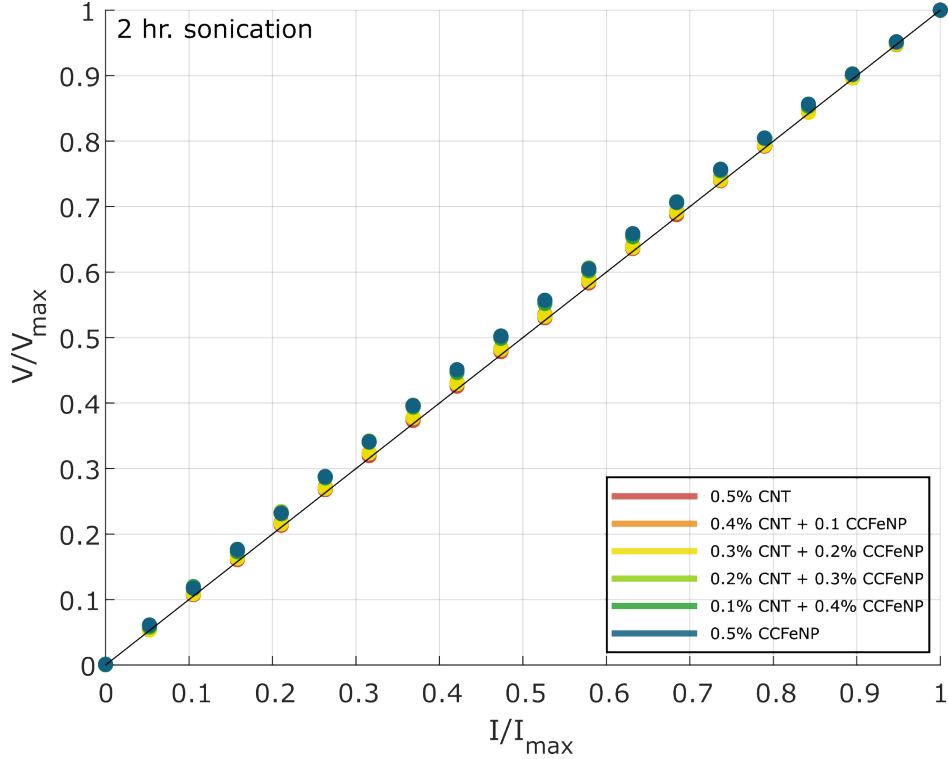
Figure 4.18. Normalised IV sweeps for each relative weight fraction as a scatter plot. A linear regression model for a perfect resistor was also plotted (shown by the black line).

time using the load and cross-sectional area of the gauge section. Axial stress versus axial strain curves were generated for each specimen group as shown in Figure 4.19. The linearity of the curves proves that the load on the specimens was below the elastic limit for the duration of the test. Elastic modulus was determined by linearly curve-fitting the loading curve for each group. The average Young's modulus for each specimen group can be found in Figure 4.21(left). We discovered that the Young's modulus of 0.1 wt.% MWCNT + 0.4 wt.% CCFeNP was greater than that of CCFeNP-only or MWCNT-only specimens. It has been shown that the addition of carbon-coated iron particles can make a matrix stiffer[106]. Thus, we can hypothesize that carbon tubes with their excellent tensile properties[107] in conjunction with iron's high stiffness lend excellent rigidity to the material system. Poisson's ratio was not determined since previous work[108] has established that little to no change is observable in this elastic quantity with changing concentrations of MWCNTs.
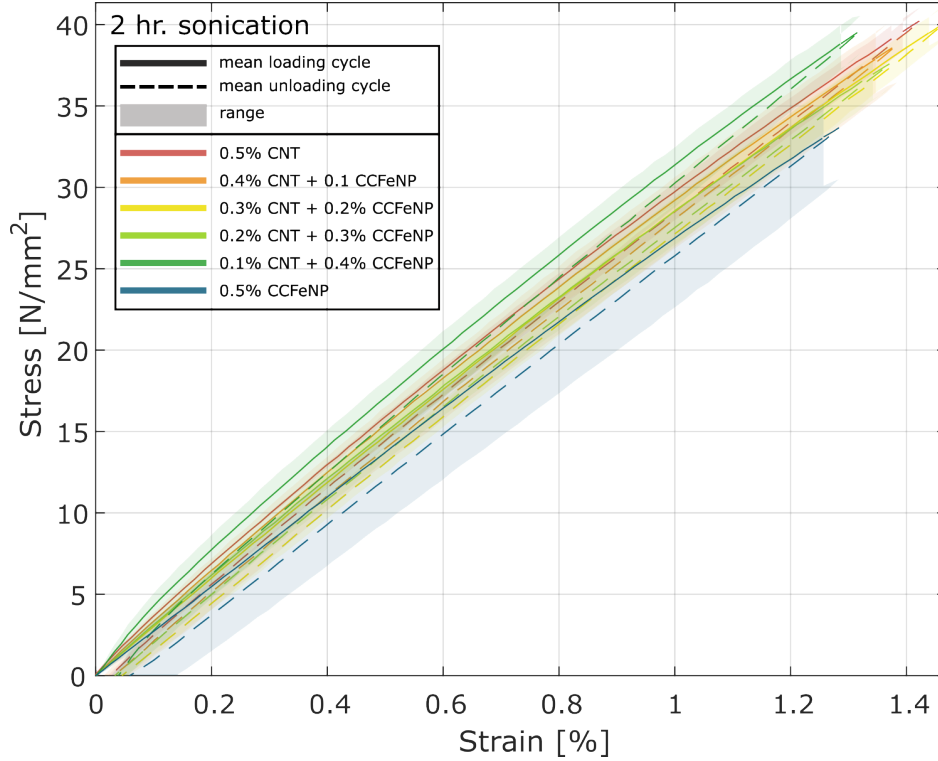
Figure 4.19. Average stress versus strain curves for each relative weight fraction. The solid lines indicate average behavior of three specimens and the shaded regions indicate the range of values.

From the measured voltage and known current one can determine the normalized change in resistance during loading as a function of measured strain. To do this, we first calculate the resistance during loading as a function of time. Next we calculate the change in resistance (ΔR). And lastly, we normalize the change in resistance against the baseline resistance (R_0). This allows us to determine the piezoresistive effect of the specimens. Peizoresistive effect is quantified by the change in electrical resistivity of a material per unit strain applied to the material. As seen in Figure 4.20, all specimens show positive piezoresistance for monotonic tensile loading, albeit it is to a much lesser extent for specimens with 0.2 wt.% or lesser quantities of MWCNTs. The gauge factor (defined by equation 4.6) was determined by a linear curve fit ($y = mx + b$) for the loading curves. It is shown in Figure 4.21(right). 0.5 wt.% MWCNT/epoxy shows the highest value of gauge factor, approximately 5.8. This may be attributed to the high concentration of electrical fillers in this group. Another interesting observation is that the gauge factor of 0.1 wt.% MWCNT + 0.4 wt.% CCFeNP/epoxy is more

than twice that of 0.2 wt.% MWCNT + 0.3 wt.% CCFeNP/epoxy. This could be because at lower MWCNT concentrations, the inter-filler distance is greater and thus deformation has a greater impact on the electron tunneling. According to the quantum theory of mechanics, electrical current can flow under certain conditions through an insulator. The insulator should have conductive elements dispersed within it. The resistance of this current, that is, tunneling resistance, depends on the closest distance between adjacent MWCNTs[109]. It can be assumed that a tensile load would increase the tunneling distance between carbon tubes. And thus, the normalized change in resistance would be more pronounced at low weight fractions of MWCNT. This phenomenon is well documented in previous work[110].

$$GF = \frac{\Delta R}{R_0}\frac{1}{\epsilon} \tag{4.6}$$
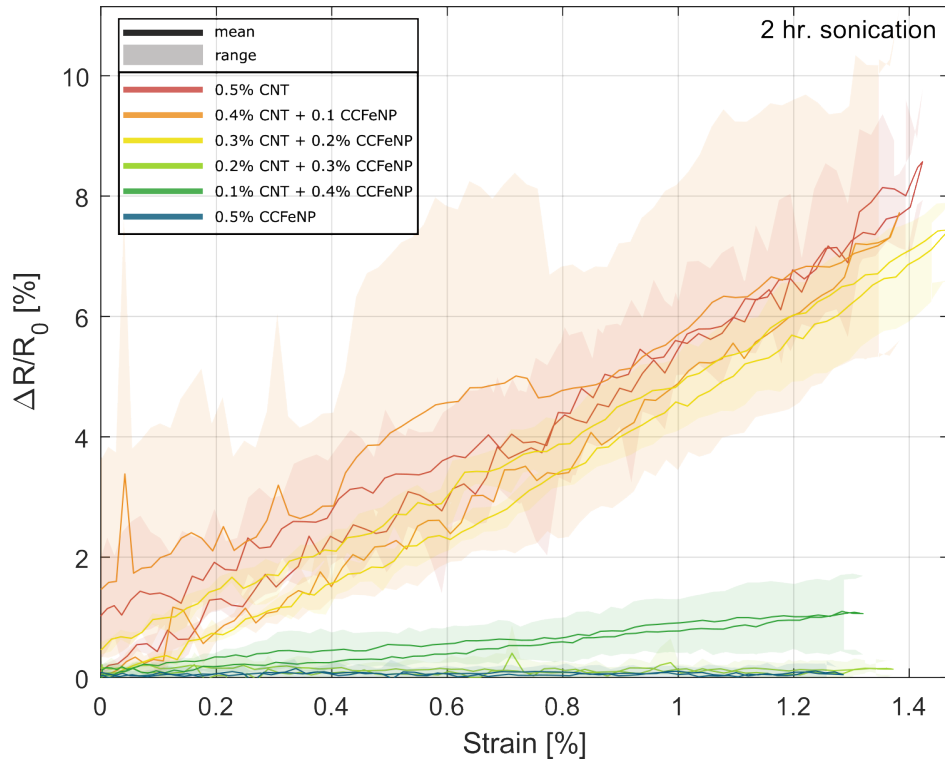
Figure 4.20. Average piezoresistance for each relative weight fraction. The solid lines indicate average behavior of three specimens and the shaded regions indicate the range of values.
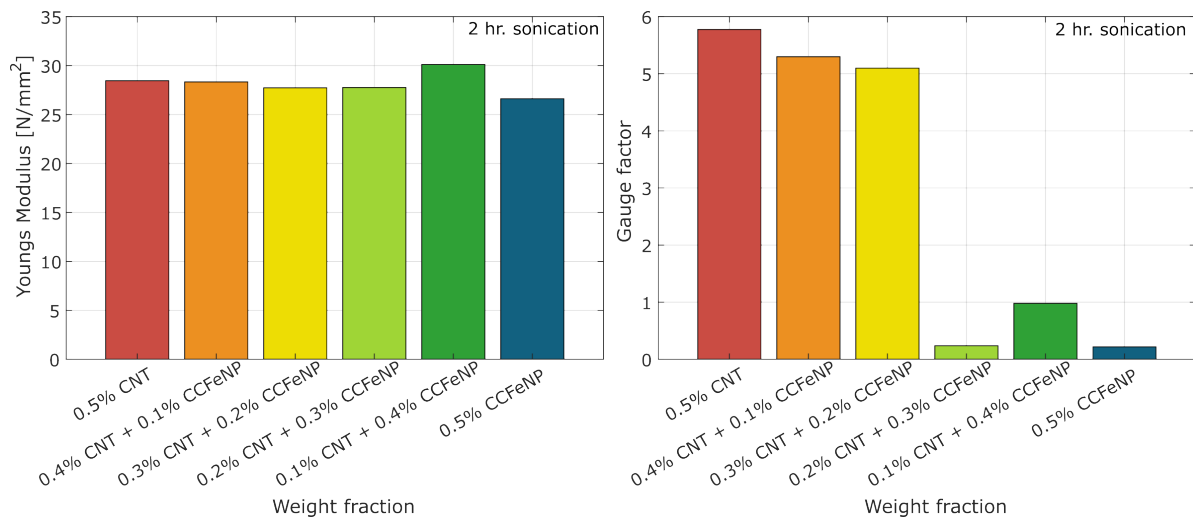
Figure 4.21. Average Young's modulus (left) and gauge factor (right) for each relative weight fraction.

5. SUMMARY, CONCLUSIONS, AND RECOMMENDATIONS FOR FUTURE WORK

To recapitulate, this work set out to understand the effects of synergistic multifunctional fillers in a structural polymer system. As engineers continue to discover wide-ranging applications of composites, it has pushed the scientific community to combine functionalities of different parts and/or materials into one. The desire to "do more with less" has served as the motivation for modified PMCs. Thus, one can find an abundance of work on polymer systems modified with a single type of nanofiller (e.g., MWCNTs, CNFs, graphene, iron oxide nanoparticles, etc.). Some work has been done on modified composites with complementary nano-fillers, that is, nanoparticles that combine to impart an improved single characteristic to the system (e.g., higher electrical conductivity). However, most exploration in this field has been one-dimensional; fillers are usually chosen to impart a single type of property such as thermal, electrical, magnetic, etc. Few have ventured to combine numerous nanofillers with distinct functionalities. There exists a gap in the field on multifiller composites with *synergistic* fillers. The authors use *synergy* to define a combination of fillers that exhibit multi-physical interactions leading to new properties. These properties cannot be attained by any individual filler in isolation but rather arise from the collective presence of all fillers in unison.

In light of the preceding paragraph, this thesis work considered a promising combination of electrical fillers (MWCNTs) and magnetic fillers (CCFeNPs) to explore synergistic effects. The two were combined in six different permutations to obtain specimen groups with different relative concentrations of fillers: 0.5 wt.% MWCNT/epoxy, 0.4 wt.% MWCNT + 0.1 wt.% CCFeNP/epoxy, 0.3 wt.% MWCNT + 0.2 wt.% CCFeNP/epoxy, 0.2 wt.% MWCNT + 0.3 wt.% CCFeNP/epoxy, 0.1 wt.% MWCNT + 0.4 wt.% CCFeNP/epoxy, and 0.5 wt.% CCFeNP/epoxy. Two batches were manufactured for each specimen group, which were sonicated for different durations. These fillers were chosen for their complementary shapes and properties; carbon nanotubes are good electrical conductors while being diamagnetic and iron nanoparticles are ferromagnetic while possessing electrical conductivity.

To understand the effect of multifiller modification on electro-magnetic properties, the resultant material system was subjected to a battery of electro-magnetic measurements looking at DC conductivity, AC conductivity, magnetic permeability, permittivity, and piezoresistance. Each test fixture required specimens of different shapes and dimensions. Thus, multiple specimens were manufactured for each test and for each specimen group. The results indicate the mean behavior of multiple specimens along with the standard deviation (in case of large data sets, ≥ 10) or range (in case of small data sets, < 10). These specific tests were chosen because of potential electro-magnetic synergistic responses between the fillers. All test procedures were designed with the intention of being non-destructive, minimizing the measurement error, and acquiring data within reasonable measurement time.

SEM images show that MWCNTs generally disperse well throughout the matrix. Some can even be seen protruding from the fracture surface. It was difficult to locate CCFeNP under the SEM and hence TEM was used to obtain a more detailed glimpse at the magnetic fillers. At a scale of 50 μm, CCFeNPs appear to cover the fracture surface relatively uniformly. When looking at the topographical view of the fracture surface, dark patches were noticed in regions where iron was located. Upon closer inspection at 17,000 magnification, we observe spherical shaped clusters of particles embedded in the matrix material.

Tests for average conductivity had interesting results as well. Even though iron is known to be electrically conductive, at 0.5 wt.% no measurable resistance or impedance magnitude was recorded from the DMM or the impedance analyzer for that specimen group. Both batches, that is, specimens sonicated for 1 and 2 hour(s), showed similar trends. Regardless of sonication time, specimens with 0.4 wt.% MWCNT + 0.1 wt.% CCFeNP had higher DC conductivity than MWCNT-only specimens. The biggest difference between the two batches was observed in the 0.1 wt.% MWCNT + 0.4 wt.% CCFeNP specimen group; longer sonication resulted in lower DC conductivity. The AC conductivity tests demonstrated the dependence of impedance magnitude on frequency. From the impedance magnitude and phase angle measured on the impedance analyzer, the real and imaginary parts of impedance were calculated. In the low frequency range ($<10^5$) Hz, specimens with 0.3 wt.% MWCNT + 0.2 wt.% CCFeNP from the first batch exhibited both high values of Z' and Z''. When sonicated for longer similar characteristics were observed in the 0.4 wt.% MWCNT + 0.1

wt.% CCFeNP group. The test apparatus also curve-fitted the electrical response of each specimen to that of a standard RLC circuit. The mean AC conductivity was computed for each specimen group as a function of frequency from the real part of impedance and the specimen dimensions. Above 1 MHz, both batches showed noisy data, although it was much more amplified for the first batch. In the sub-MHz range, the first batch produced results similar to those seen in DC conductivity. However, the results of the second batch deviated from those seen in DC conductivity. Here, both 0.5 wt.% MWCNT/epoxy and 0.1 wt.% MWCNT + 0.4 wt.% CCFeNP/epoxy had very high conductivity.

Next, the magnetic permeability was determined by recording the magnetic moment of three cylindrical specimens from each group in an applied magnetic field that ranged from +30,000 Oe to -30,000 Oe. As anticipated, the value of average magnetization increased with increasing quantities of ferromagnetic material. However, one interesting observation was that the addition of carbon in small quantities to iron, that is, the 0.1 wt.% MWCNT + 0.4 wt.% CCFeNP group had higher saturation magnetization than 0.5 wt.% CCFeNP by approximately 1.3 times, which may be indicative of a synergistic interaction. The coercivity and retentivity were also determined from the resulting hysteresis curves. While retentivity showed trends similar to those seen in saturation magnetization, coercivity increased with increasing quantities of iron, independent of the amount of carbon in the specimens.

Another quantity of interest was the relative dielectric constant of the material system. Employing the non-contacting electrode method on the Keysight dielectric test fixture, the series capacitance and dissipation factor were measured for five specimens from each group as a function of frequency on an impedance analyzer. The results show that while the average dielectric constant decreased with increasing frequency, the dissipation factor increased with increasing frequency. When analyzing these quantities across different specimens, the 0.3 wt.% MWCNT + 0.2 wt.% CCFeNP group had the highest dielectric constant as well as dissipation factor.

The last test was designed to study both mechanical as well as piezoresistive characteristics. This was done by applying a simple monotonic load on dogbone shaped specimens up to 1% engineering strain while the resultant strain and change in resistance across the gauge section was measured as a function of time. The corresponding stress-strain curves were

generated for all specimens for both the loading and unloading cycle. All curves were linear. Specimens with 0.1 wt.% MWCNT + 0.4 wt.% CCFeNP had the highest slope, that is, the largest value of Young's modulus, (about 30 MPa). This was followed closely by the 0.5 wt.% CCFeNP group at about 28 MPa. However, this was not the trend seen in the gauge factor. 0.5 wt.% MWCNT/epoxy had the highest change in resistance per unit strain (about 5.8 during loading). However, the largest change in pre-experimental and post-experimental resistance was observed for the 0.1 wt.% MWCNT + 0.4 wt.% CCFeNP group (about 750 kΩ).

5.1 Conclusions

Following the methodology for manufacturing and specimen preparation described in previous sections, these results show that the addition of even 0.1 wt.% CCFeNP to MWC-NTs significantly increases the conductivity of the composite while also imparting magnetic properties. Additionally, it was observed that the composite's magnetic properties (i.e., saturation magnetization and susceptibility) were enhanced with the addition of 0.1 wt.% MWCNT to 0.4 wt.% CCFeNP but decreased below 0.4 wt.% CCFeNP. The permittivity results indicate that while 0.3 wt.% MWCNT + 0.2 wt.% CCFeNP/epoxy has low conductivity, this combination of fillers has significant electric charge storage properties, especially in the sub-MHz range. And lastly, from the stress-strain curves, one can conclude that the combination of carbon particles and iron nanoparticles aids the stiffness to be higher than that of single-filler specimens. However, gauge factor is largely dependent on the amount of carbon nanotubes in the material system.

All material properties that we tested for (electrical conductivity, permeability, permittivity, and piezoresistance) gave rise to noteworthy findings. The findings point towards the indication that the properties of this material system could be borne from the synergy of the two fillers. At the very least, certain attributes cannot be credited to any single filler alone. However, more wide-ranging and comprehensive tests need to be performed to reach definitive experimental conclusions. Computational modelling of the system could be employed to explain the mechanisms of interactions between the fillers.

5.2 Future Work

While this thesis has successfully established baseline results for polymer composites incorporated with synergistic electromagnetic fillers, there is much ground yet to be covered in the field of synergistic multifunctional modification of composites. Listed below are a few paths that could carry this work forward.

1. The preliminary work covered here needs to be expanded further to include test methodologies which can uncover other modes of synergy. For example, the authors are currently trying to establish the presence of magnetoresistance in this material system. Magnetoresistance can be defined as the change in resistance corresponding to an applied electric field because of the effects of a simultaneously applied magnetic field. While this phenomenon has been well documented in ferromagnetic materials, it would be interesting to see how the presence of a diamagnetic material would influence it. Work done on iron-filled carbon nanotubes could also serve as a basis[84].

2. This work studies a polymer based material system with a total filler weight fraction at 0.5 wt.%. Future work can carry this forward by exploring higher filler weight fractions (maybe up to 2.5 wt.%) since MWCNTs show significant changes in conductivity above this weight fraction as well.

3. When looking at iron-only specimens, the concentration of CCFeNPs was insufficient to establish a well-connected electrical network. Iron is a well-known conductor of electricity. Thus, it would be helpful to establish the percolation threshold of CCFeNP, understand the changes in conductivity near this value, and how it affects synergy with MWCNTs.

4. And lastly, more characterization tests need to performed. To fully integrate this system in any real-world application, one would have to characterize the material under other forms of external loading (for example, tensile loading with an applied magnetic field).

6. ACKNOWLEDGEMENTS

A. MEASUREMENT ERROR ANALYSIS FOR PERMITTIVITY TESTS

A.1 Error factor using non-contacting electrode method

There are some sources of error when using the LCR meter in conjunction with the dielectric test fixture. This includes measurement error of test material's thickness, parallelism and flatness of electrodes and test materials, and error in gap between electrodes. Error in measuring t_a could arise from the micrometer. This error can be reduced by performing multiple measurements along the thickness of the test material with an independent micrometer. When parallelism and flatness of the electrodes are not perfect, an air film between surfaces of the electrode and the test material can cause error. This error can be reduced by ensuring proper specimen preparation, that is, parallel and flat faces on the specimen. If the scale of the micrometer differs from the actual distance between the electrodes, an error can be introduced in measuring t_g. All these sources of error can be reduced by the following procedure

1. Measure the capacitance at three different electrode distances.

2. Calculate the theoretical capacitance value of each distance. The theoretical capacitance value Ct can be obtained by equation A.1 where C_t is the theoretical capacitance in F, ε_a is the dielectric constant of air (=1.00059), $\varepsilon_0 = 8.854 10^{-12} [F/m]$, α_a is the effective area coefficient of electrode when the electrode distance is t_{set}, and t_{set} is the reading value of the electrode distance on the micrometer in m.

$$C_t = \varepsilon_a \times \varepsilon_0 \times \frac{\pi \times (d/2)^2}{t_{set}} \times \alpha_a \tag{A.1}$$

3. Calculate the equivalent distance error at each electrode distance. The equivalent distance error of each electrode distance Δt_e can be obtained by equation A.2 where C_m is the measured capacitance value in F.

$$\Delta t_e = (\frac{C_t}{C_m} - 1) \times t_{set} \tag{A.2}$$

4. Average the equivalent distance error

Stray capacitance at the electrodes edges causes error in the measured values C_{s1} and C_{s2}. To reduce this error, divide capacitance values by the effective area constants. The compensated dielectric constant can be obtained as given by equation A.3 where α_a and α_b are the effective area constants.

$$\varepsilon_r = \frac{1}{1 - \left(1 - \frac{C_{s1}}{C_{s2}} \times \frac{\alpha_b}{\alpha_a}\right) \times \frac{t_{eq}}{t_a}} \tag{A.3}$$

REFERENCES

[1]   C. S. P.E. Irving, *Polymer Composites in the Aerospace Industry*. Elsevier, 2014.

[2]   L. Lin, S. Park, Y. Kim, *et al.*, "Wearable and stretchable conductive polymer composites for strain sensors: How to design a superior one?" *Nano Materials Science*, 2022.

[3]   S. Nauman, "Piezoresistive sensing approaches for structural health monitoring of polymer compositesa review," *Eng*, vol. 2, no. 2, pp. 197–226, 2021.

[4]   T. Vijaybabu, T. Ramesh, S. Pandipati, *et al.*, "High thermal conductivity polymer composites fabrication through conventional and 3d printing processes: State-of-the-art and future trends," *Macromolecular Materials and Engineering*, p. 2 300 001, 2023.

[5]   A. Adhikari, J. Nath, S. De, J. T. Orasugh, and D. Chattopadhyay, "Polymer composites for gas sensors," in *Polymeric Nanocomposite Materials for Sensor Applications*, Elsevier, 2023, pp. 173–198.

[6]   M. Ramakrishnan, G. Rajan, Y. Semenova, and G. Farrell, "Overview of fiber optic sensor technologies for strain/temperature sensing applications in composite materials," *Sensors*, vol. 16, no. 1, p. 99, 2016.

[7]   S. Masmoudi, A. El Mahi, and S. Turki, "Fatigue behaviour and structural health monitoring by acoustic emission of e-glass/epoxy laminates with piezoelectric implant," *Applied Acoustics*, vol. 108, pp. 50–58, 2016.

[8]   P.-C. Ma, M.-Y. Liu, H. Zhang, *et al.*, "Enhanced electrical conductivity of nanocomposites containing hybrid fillers of carbon nanotubes and carbon black," *ACS applied materials & interfaces*, vol. 1, no. 5, pp. 1090–1096, 2009.

[9]   D. J. Kim, M. J. Jo, and S. Y. Nam, "A review of polymer–nanocomposite electrolyte membranes for fuel cell application," *Journal of Industrial and Engineering Chemistry*, vol. 21, pp. 36–52, 2015.

[10]   Q. Wang and L. Zhu, "Polymer nanocomposites for electrical energy storage," *Journal of Polymer Science Part B: Polymer Physics*, vol. 49, no. 20, pp. 1421–1429, 2011.

[11]   S. Srivastava, M. Haridas, and J. Basu, "Optical properties of polymer nanocomposites.," *Bulletin of Materials Science*, vol. 31, no. 3, 2008.

[12] A. Z. M. Badruddoza, Z. B. Z. Shawon, W. J. D. Tay, K. Hidajat, and M. S. Uddin, "Fe3o4/cyclodextrin polymer nanocomposites for selective heavy metals removal from industrial wastewater," *Carbohydrate polymers*, vol. 91, no. 1, pp. 322–332, 2013.

[13] K. Schulte and C. Baron, "Load and failure analyses of cfrp laminates by means of electrical resistivity measurements," *Composites science and technology*, vol. 36, no. 1, pp. 63–76, 1989.

[14] J. Du and H.-M. Cheng, "The fabrication, properties, and uses of graphene/polymer composites," *Macromolecular Chemistry and Physics*, vol. 213, no. 10-11, pp. 1060–1077, May 2012.

[15] N. Sakharova, A. Pereira, J. Antunes, C. Brett, and J. Fernandes, "Mechanical characterization of single-walled carbon nanotubes: Numerical simulation study," *Composites Part B: Engineering*, vol. 75, pp. 73–85, Jun. 2015.

[16] L. Kong and W. Chen, "Carbon nanotube and graphene-based bioinspired electrochemical actuators," *Advanced Materials*, vol. 26, no. 7, pp. 1025–1043, Dec. 2013.

[17] K.-Y. Chan, B. Jia, H. Lin, N. Hameed, J.-H. Lee, and K.-T. Lau, "A critical review on multifunctional composites as structural capacitors for energy storage," *Composite Structures*, vol. 188, pp. 126–142, 2018.

[18] D. Fam, A. Palaniappan, A. Tok, B. Liedberg, and S. Moochhala, "A review on technological aspects influencing commercialization of carbon nanotube sensors," *Sensors and Actuators B: Chemical*, vol. 157, no. 1, pp. 1–7, Sep. 2011.

[19] L. Dai, D. W. Chang, J.-B. Baek, and W. Lu, "Carbon nanomaterials for advanced energy conversion and storage," *Small*, vol. 8, no. 8, pp. 1130–1166, Mar. 2012.

[20] C. W. Tan, K. H. Tan, Y. T. Ong, A. R. Mohamed, S. H. S. Zein, and S. H. Tan, "Energy and environmental applications of carbon nanotubes," *Environmental Chemistry Letters*, vol. 10, no. 3, pp. 265–273, Feb. 2012.

[21] D. S. A. D. Focatiis, D. Hull, and A. Sánchez-Valencia, "Roles of prestrain and hysteresis on piezoresistance in conductive elastomers for strain sensor applications," *Plastics, Rubber and Composites*, vol. 41, no. 7, pp. 301–309, Sep. 2012.

[22] N. Luo, W. Dai, C. Li, *et al.*, "Flexible piezoresistive sensor patch enabling ultralow power cuffless blood pressure measurement," *Advanced Functional Materials*, vol. 26, no. 8, pp. 1178–1187, Dec. 2015.

[23]   T. J. Kang, A. Choi, D.-H. Kim, *et al.*, "Electromechanical properties of CNT-coated cotton yarn for electronic textile applications," *Smart Materials and Structures*, vol. 20, no. 1, p. 015 004, Dec. 2010.

[24]   J. Hwang, J. Jang, K. Hong, *et al.*, "Poly(3-hexylthiophene) wrapped carbon nanotube/poly(dimethylsiloxane) composites for use in finger-sensing piezoresistive pressure sensors," *Carbon*, vol. 49, no. 1, pp. 106–110, Jan. 2011.

[25]   Y.-J. Kim, J. Y. Cha, H. Ham, H. Huh, D.-S. So, and I. Kang, "Preparation of piezoresistive nano smart hybrid material based on graphene," *Current Applied Physics*, vol. 11, no. 1, S350–S352, 2011.

[26]   M.-Y. Cheng, C.-M. Tsao, Y.-Z. Lai, and Y.-J. Yang, "The development of a highly twistable tactile sensing array with stretchable helical electrodes," *Sensors and Actuators A: Physical*, vol. 166, no. 2, pp. 226–233, 2011.

[27]   T. Yamada, Y. Hayamizu, Y. Yamamoto, *et al.*, "A stretchable carbon nanotube strain sensor for human-motion detection," *Nature nanotechnology*, vol. 6, no. 5, pp. 296–301, 2011.

[28]   N. Li, S. Oida, G. S. Tulevski, *et al.*, "Efficient and bright organic light-emitting diodes on single-layer graphene electrodes," *Nature communications*, vol. 4, no. 1, p. 2294, 2013.

[29]   F. Avilés, A. I. Oliva-Avilés, and M. Cen-Puc, "Piezoresistivity, strain, and damage self-sensing of polymer composites filled with carbon nanostructures," *Advanced Engineering Materials*, vol. 20, no. 7, p. 1 701 159, 2018.

[30]   V. Boggarapu, R. Gujjala, S. Ojha, *et al.*, "State of the art in functionally graded materials," *Composite Structures*, vol. 262, p. 113 596, Apr. 2021.

[31]   D. Jha, T. Kant, and R. Singh, "A critical review of recent research on functionally graded plates," *Composite Structures*, vol. 96, pp. 833–849, Feb. 2013.

[32]   K. Beena and U. Parvathy, "Linear static analysis of functionally graded plate using spline finite strip method," *Composite Structures*, vol. 117, pp. 309–315, Nov. 2014.

[33]   M. Niino, K. Kisara, and M. Mori, "Feasibility study of FGM technology in space solar power systems (SSPS)," *Materials Science Forum*, vol. 492-493, pp. 163–170, Aug. 2005.

[34] F. Watari, A. Yokoyama, M. Omori, *et al.*, "Biocompatibility of materials and development to functionally graded implant for bio-medical application," *Composites Science and Technology*, vol. 64, no. 6, pp. 893–908, May 2004.

[35] A. Pasha and R. B.M, "Functionally graded materials (FGM) fabrication and its potential challenges &amp applications," *Materials Today: Proceedings*, vol. 52, pp. 413–418, 2022.

[36] I. Bharti, N. Gupta, and K. M. Gupta, "Novel applications of functionally graded nano, optoelectronic and thermoelectric materials," *International Journal of Materials, Mechanics and Manufacturing*, pp. 221–224, 2013.

[37] X. Wang, X. Fu, and D. D. L. Chung, "Strain sensing using carbon fiber," *Journal of Materials Research*, vol. 14, no. 3, pp. 790–802, 1999.

[38] J. Wen, Z. Xia, and F. Choy, "Damage detection of carbon fiber reinforced polymer composites via electrical resistance measurement," *Composites Part B: Engineering*, vol. 42, no. 1, pp. 77–86, Jan. 2011.

[39] T. Carlson, D. Ordéus, M. Wysocki, and L. E. Asp, "CFRP structural capacitor materials for automotive applications," *Plastics, Rubber and Composites*, vol. 40, no. 6-7, pp. 311–316, Sep. 2011.

[40] H. Zhu, K. Fu, B. Yang, and Y. Li, "Nickel-coated nylon sandwich film for combination of lightning strike protection and electromagnetic interference shielding of CFRP composite," *Composites Science and Technology*, vol. 207, p. 108 675, May 2021.

[41] G. Williams, I. Bond, and R. Trask, "Compression after impact assessment of self-healing CFRP," *Composites Part A: Applied Science and Manufacturing*, vol. 40, no. 9, pp. 1399–1406, Sep. 2009.

[42] D. D. Chung, "Composites get smart," *Materials Today*, vol. 5, no. 1, pp. 30–35, Jan. 2002.

[43] G. J. Gallo and E. T. Thostenson, "Electrical characterization and modeling of carbon nanotube and carbon fiber self-sensing composites for enhanced sensing of microcracks," *Materials today communications*, vol. 3, pp. 17–26, 2015.

[44] C. Joseph and C. Viney, "Electrical resistance curing of carbon-fibre/epoxy composites," *Composites Science and Technology*, vol. 60, no. 2, pp. 315–319, 2000.

[45] S. H. McKnight, S. T. Holmes, J. W. Gillespie Jr, C. L. Lambing, and J. M. Marinelli, "Scaling issues in resistance-welded thermoplastic composite joints," *Advances in Polymer Technology: Journal of the Polymer Processing Institute*, vol. 16, no. 4, pp. 279–295, 1997.

[46] J. M. Kim, Y. Lee, M. G. Jang, C. Han, and W. N. Kim, "Electrical conductivity and EMI shielding effectiveness of polyurethane foam-conductive filler composites," *Journal of Applied Polymer Science*, vol. 134, no. 5, Sep. 2016.

[47] X. Luo and D. Chung, "Carbon-fiber/polymer-matrix composites as capacitors," *Composites Science and Technology*, vol. 61, no. 6, pp. 885–888, 2001.

[48] J.-P. Peng, H. Zhang, L.-C. Tang, Y. Jia, and Z. Zhang, "Dielectric properties of carbon nanotubes/epoxy composites," *Journal of Nanoscience and Nanotechnology*, vol. 13, no. 2, pp. 964–969, 2013.

[49] A. Pardo, M. Gómez-Florit, S. Barbosa, P. Taboada, R. M. A. Domingues, and M. E. Gomes, "Magnetic nanocomposite hydrogels for tissue engineering: Design concepts and remote actuation strategies to control cell fate," *ACS Nano*, vol. 15, no. 1, pp. 175–209, 2021.

[50] K. K. Mohammad Sadegh Amini-Fazl Reza Mohammadi, "5fluorouracil loaded chitosan/polyacrylic acid/fe3o4 magnetic nanocomposite hydrogel as a potential anticancer drug delivery system.," vol. 132, pp. 506–513, 2019.

[51] M. Yan, Q. Liang, W. Wan, Q. Han, S. Tan, and M. Ding, "Amino acid-modified graphene oxide magnetic nanocomposite for the magnetic separation of proteins," *RSC Advances*, vol. 7, no. 48, pp. 30 109–30 117, 2017.

[52] G. C. Lavorato, R. Das, J. A. Masa, M.-H. Phan, and H. Srikanth, "Hybrid magnetic nanoparticles as efficient nanoheaters in biomedical applications," *Nanoscale Advances*, vol. 3, no. 4, pp. 867–888, 2021.

[53] A. Sood, V. Arora, J. Shah, R. Kotnala, and T. K. Jain, "Multifunctional gold coated iron oxide core-shell nanoparticles stabilized using thiolated sodium alginate for biomedical applications," *Materials Science and Engineering: C*, vol. 80, pp. 274–281, Nov. 2017.

[54] S. Saeedirad, J. Seyed-Yazdi, and S. H. Hekmatara, "Decorating untreated carbon nanotubes with fe3o4@sio2 nanoparticles and its microwave absorption property," *Journal of Alloys and Compounds*, vol. 793, pp. 590–598, 2019, ISSN: 0925-8388.

[55] C. Jin, Y. Wang, H. Wei, *et al.*, "Magnetic iron oxide nanoparticles coated by hierarchically structured silica: A highly stable nanocomposite system and ideal catalyst support," *Journal of Materials Chemistry A*, vol. 2, no. 29, p. 11 202, 2014.

[56] H. Wang, J. Shen, Y. Li, *et al.*, "Porous carbon protected magnetite and silver hybrid nanoparticles: Morphological control, recyclable catalysts, and multicolor cell imaging," *ACS Applied Materials &amp Interfaces*, vol. 5, no. 19, pp. 9446–9453, 2013.

[57] J. Li, L. Zheng, H. Cai, *et al.*, "Polyethyleneimine-mediated synthesis of folic acid-targeted iron oxide nanoparticles for in vivo tumor mr imaging," *Biomaterials*, vol. 34, no. 33, pp. 8382–8392, 2013.

[58] J. Durán, J. Arias, V. Gallardo, and A. Delgado, "Magnetic colloids as drug vehicles," *Journal of Pharmaceutical Sciences*, vol. 97, no. 8, pp. 2948–2983, 2008.

[59] P. Moradi, B. Zarei, Y. A. Tyula, and M. Nikoorazm, "Novel neodymium complex on MCM-41 magnetic nanocomposite as a practical, selective, and returnable nanocatalyst in the synthesis of tetrazoles with antifungal properties in agricultural," *Applied Organometallic Chemistry*, vol. 37, no. 4, 2023.

[60] Q.-Q. Dai, J.-L. Ren, F. Peng, X.-F. Chen, C.-D. Gao, and R.-C. Sun, "Synthesis of acylated xylan-based magnetic fe3o4 hydrogels and their application for h2o2 detection," *Materials*, vol. 9, no. 8, p. 690, 2016.

[61] M. Torres-Lugo and C. Rinaldi, "Thermal potentiation of chemotherapy by magnetic nanoparticles," *Nanomedicine*, vol. 8, no. 10, pp. 1689–1707, 2013.

[62] T. R. Sathe, A. Agrawal, and S. Nie, "Mesoporous silica beads embedded with semiconductor quantum dots and iron oxide nanocrystals: dual-function microcarriers for optical encoding and magnetic separation," *Analytical Chemistry*, vol. 78, no. 16, pp. 5627–5632, 2006.

[63] Q. Ze, X. Kuang, S. Wu, *et al.*, "Magnetic shape memory polymers with integrated multifunctional shape manipulation," *Advanced Materials*, vol. 32, no. 4, p. 1 906 657, 2020.

[64] L. S. Novelino, Q. Ze, S. Wu, G. H. Paulino, and R. Zhao, "Untethered control of functional origami microrobots with distributed actuation," *Proceedings of the National Academy of Sciences*, vol. 117, no. 39, pp. 24 096–24 101, 2020.

[65] T. Hu, S. Xuan, L. Ding, and X. Gong, "Stretchable and magneto-sensitive strain sensor based on silver nanowire-polyurethane sponge enhanced magnetorheological elastomer," *Materials & Design*, vol. 156, pp. 528–537, 2018.

[66] X. Xu, H. Li, Q. Zhang, *et al.*, "Self-sensing, ultralight, and conductive 3d graphene/-iron oxide aerogel elastomer deformable in a magnetic field," *ACS nano*, vol. 9, no. 4, pp. 3969–3977, 2015.

[67] G. Yun, S.-Y. Tang, S. Sun, *et al.*, "Liquid metal-filled magnetorheological elastomer with positive piezoconductivity," *Nature communications*, vol. 10, no. 1, p. 1300, 2019.

[68] A. Alfadhel and J. Kosel, "Magnetic nanocomposite cilia tactile sensor," 2015.

[69] G. Wypych, "Handbook of fillers," 1999.

[70] M. M. Thwe and K. Liao, "Durability of bamboo-glass fiber reinforced polymer matrix hybrid composites," *Composites science and technology*, vol. 63, no. 3-4, pp. 375–387, 2003.

[71] S.-Y. Fu, G. Xu, and Y.-W. Mai, "On the elastic modulus of hybrid particle/short-fiber/polymer composites," *Composites Part B: Engineering*, vol. 33, no. 4, pp. 291–299, 2002.

[72] U. Szeluga, B. Kumanek, and B. Trzebicka, "Synergy in hybrid polymer/nanocarbon composites. a review," *Composites Part A: Applied Science and Manufacturing*, vol. 73, pp. 204–231, 2015.

[73] S.-Y. Yang, W.-N. Lin, Y.-L. Huang, *et al.*, "Synergetic effects of graphene platelets and carbon nanotubes on the mechanical and thermal properties of epoxy composites," *Carbon*, vol. 49, no. 3, pp. 793–803, 2011.

[74] Z.-M. Dang, K. Shehzad, J.-W. Zha, *et al.*, "Complementary percolation characteristics of carbon fillers based electrically percolative thermoplastic elastomer composites," *Composites science and technology*, vol. 72, no. 1, pp. 28–35, 2011.

[75] H. Deng, T. Skipa, E. Bilotti, *et al.*, "Preparation of high-performance conductive polymer fibers through morphological control of networks formed by nanofillers," *Advanced Functional Materials*, vol. 20, no. 9, pp. 1424–1432, 2010.

[76]   T. A. Kim, H. S. Kim, S. S. Lee, and M. Park, "Single-walled carbon nanotube/silicone rubber composites for compliant electrodes," *Carbon*, vol. 50, no. 2, pp. 444–449, 2012.

[77]   T. Connolly, R. C. Smith, Y. Hernandez, Y. Gun'ko, J. N. Coleman, and J. D. Carey, "Carbon-nanotube–polymer nanocomposites for field-emission cathodes," *small*, vol. 5, no. 7, pp. 826–831, 2009.

[78]   S. Sharma, P. Kumar, and R. Chandra, "Mechanical and thermal properties of graphene–carbon nanotube-reinforced metal matrix composites: A molecular dynamics study," *Journal of Composite Materials*, vol. 51, no. 23, pp. 3299–3313, 2017.

[79]   S. Morimune-Moriya, T. Goto, and T. Nishino, "Effect of aspect ratio of graphene oxide on properties of poly (vinyl alcohol) nanocomposites," *Nanocomposites*, vol. 5, no. 3, pp. 84–93, 2019.

[80]   J. Li, P.-S. Wong, and J.-K. Kim, "Hybrid nanocomposites containing carbon nanotubes and graphite nanoplatelets," *Materials Science and Engineering: A*, vol. 483, pp. 660–663, 2008.

[81]   A. Das, G. R. Kasaliwal, R. Jurk, *et al.*, "Rubber composites based on graphene nanoplatelets, expanded graphite, carbon nanotubes and their combination: A comparative study," *Composites Science and Technology*, vol. 72, no. 16, pp. 1961–1967, 2012.

[82]   S. Zhang, S. Yin, C. Rong, P. Huo, Z. Jiang, and G. Wang, "Synergistic effects of functionalized graphene and functionalized multi-walled carbon nanotubes on the electrical and mechanical properties of poly (ether sulfone) composites," *European polymer journal*, vol. 49, no. 10, pp. 3125–3134, 2013.

[83]   O. Lozitsky, L. Vovchenko, L. Matzui, Y. Milovanov, and V. Garashchenko, "Electrical properties of epoxy composites with carbon nanotubes, mixed with tio2 or fe particles," *Applied Nanoscience*, vol. 11, no. 6, pp. 1827–1837, 2021.

[84]   S. Hudziak, A. Darfeuille, R. Zhang, *et al.*, "Magnetoresistive phenomena in an fe-filled carbon nanotube/elastomer composite," *Nanotechnology*, vol. 21, no. 12, p. 125 505, 2010.

[85]   M. Engel, Y. Hadar, S. Belkin, X. Lu, M. Elimelech, and B. Chefetz, "Bacterial inactivation by a carbon nanotubeiron oxide nanocomposite: A mechanistic study usingie. coli/imutants," *Environmental Science: Nano*, vol. 5, no. 2, pp. 372–380, 2018.

[86]   F. Mousavi and A. A. Taherpour, "A carbon nanotube-iron (III) oxide nanocomposite as a cathode in dye-sensitized solar cells: Computational modeling and electrochemical investigations," *Electrochimica Acta*, vol. 318, pp. 617–624, Sep. 2019.

[87]   C. Huiqun, Z. Meifang, and L. Yaogang, "Novel carbon nanotube iron oxide magnetic nanocomposites," *Journal of magnetism and magnetic materials*, vol. 305, no. 2, pp. 321–324, 2006.

[88]   L. Xing, Y. Chen, Y. Yang, *et al.*, "Incorporation of fexoy nanoparticles into 3d interlinked porous carbon nanofiber networks to synergistically enhance the electrical insulation, electromagnetic wave absorbing/shielding performance and thermal conductivity," *Chemical Engineering Journal*, p. 143 952, 2023.

[89]   V. K. Sharma, T. J. McDonald, H. Kim, and V. K. Garg, "Magnetic graphene–carbon nanotube iron nanocomposites as adsorbents and antibacterial agents for water purification," *Advances in colloid and interface science*, vol. 225, pp. 229–240, 2015.

[90]   Quantum Design, *Magnetic property measurement system, mpms 3, 15th edition*, 2016.

[91]   Keysight Technologies, *Keysight 16451b dielectric test fixture, 7th edition*, Operation and service manual, 2023.

[92]   F. Wang, L. T. Drzal, Y. Qin, and Z. Huang, "Processing and characterization of high content multilayer graphene/epoxy composites with high electrical conductivity," *Polymer Composites*, vol. 37, no. 9, pp. 2897–2906, 2016.

[93]   A. Kumar, K. Sharma, and A. R. Dixit, "Carbon nanotube-and graphene-reinforced multiphase polymeric composites: Review on their properties and applications," *Journal of Materials Science*, vol. 55, no. 7, pp. 2682–2724, 2020.

[94]   M. J. Shea, J. Wang, J. T. Flach, M. T. Zanni, and M. S. Arnold, "Less severe processing improves carbon nanotube photovoltaic performance," *APL Materials*, vol. 6, no. 5, p. 056 104, 2018.

[95]   K. Yan, Q. Xue, Q. Zheng, and L. Hao, "The interface effect of the effective electrical conductivity of carbon nanotube composites," *Nanotechnology*, vol. 18, no. 25, p. 255 705, 2007.

[96]   Y. Wang, S. Lu, W. He, *et al.*, "Modeling and characterization of the electrical conductivity on metal nanoparticles/carbon nanotube/polymer composites," *Scientific Reports*, vol. 12, no. 1, p. 10 448, 2022.

[97]   D.-X. Chen, J. A. Brug, and R. B. Goldfarb, "Demagnetizing factors for cylinders," *IEEE Transactions on magnetics*, vol. 27, no. 4, pp. 3601–3619, 1991.

[98]   N. A. Spaldin, *Magnetic materials: fundamentals and applications.* Cambridge university press, 2010.

[99]   O. Cespedes, M. Ferreira, S. Sanvito, M. Kociak, and J. Coey, "Contact induced magnetism in carbon nanotubes," *Journal of Physics: Condensed Matter*, vol. 16, no. 10, p. L155, 2004.

[100] J. Jiao, S. Seraphin, X. Wang, and J. C. Withers, "Preparation and properties of ferromagnetic carbon-coated fe, co, and ni nanoparticles," *Journal of Applied Physics*, vol. 80, no. 1, pp. 103–108, 1996.

[101] Keysight Technologies, *Basics of measuring the dielectric properties of materials*, Application note, 2020.

[102] Y. Song, T. W. Noh, S.-I. Lee, and J. R. Gaines, "Experimental study of the three-dimensional ac conductivity and dielectric constant of a conductor-insulator composite near the percolation threshold," *Physical Review B*, vol. 33, no. 2, p. 904, 1986.

[103] T. Hanai and K. Sekine, "Theory of dielectric relaxations due to the interfacial polarization for two-component suspensions of spheres," *Colloid and Polymer Science*, vol. 264, pp. 888–895, 1986.

[104] X. Guo, D. Yu, Y. Gao, Q. Li, W. Wan, and Z. Gao, "Dielectric properties of filled carbon nanotubes/epoxy composites with high dielectric constant," in *2006 1st IEEE International Conference on Nano/Micro Engineered and Molecular Systems*, IEEE, 2006, pp. 295–298.

[105] K. Ghosh, S. K. Srivastava, and S. Puravankara, "Nanostructured zro2/mwcnt hybrid materials: Fabrication, characterization and applications in shielding of electromagnetic pollution," *Journal of Nanoscience and Nanotechnology*, vol. 19, no. 6, pp. 3367–3375, 2019.

[106] I. Dulinska-Molak, A. Chlanda, J. Li, *et al.*, "The influence of carbon-encapsulated iron nanoparticles on elastic modulus of living human mesenchymal stem cells examined by atomic force microscopy," *Micron*, vol. 108, pp. 41–48, 2018.

[107] A. Takakura, K. Beppu, T. Nishihara, *et al.*, "Strength of carbon nanotubes depends on their chemical structures," *Nature communications*, vol. 10, no. 1, p. 3040, 2019.

[108] M.-K. Yeh, N.-H. Tai, and D.-S. Lin, "Vibration characteristics of multi-walled carbon nanotubes/epoxy composites beam," *Procedia Engineering*, vol. 79, pp. 244–248, 2014.

[109] A. Alizadeh Sahraei, M. Ayati, M. Baniassadi, D. Rodrigue, M. Baghani, and Y. Abdi, "Ac and dc electrical behavior of mwcnt/epoxy nanocomposite near percolation threshold: Equivalent circuits and percolation limits," *Journal of Applied Physics*, vol. 123, no. 10, p. 105 109, 2018.

[110] C. Li, E. T. Thostenson, and T.-W. Chou, "Dominant role of tunneling resistance in the electrical conductivity of carbon nanotube–based composites," *Applied Physics Letters*, vol. 91, no. 22, p. 223 114, 2007.